USGS
science for a changing world

Smithsonian Institution

U.S. Naval Research Laboratory

GEOLOGIC INVESTIGATIONS SERIES MAP I–2800
THIS DYNAMIC PLANET—
World map of volcanoes, earthquakes, impact craters, and plate tectonics
By Tom Simkin, R.I. Tilling, P.R. Vogt, S.H. Kirby, Paul Kimberly, and D.B. Stewart
2006

I. New Crust Grows at Divergent (Spreading) Boundaries

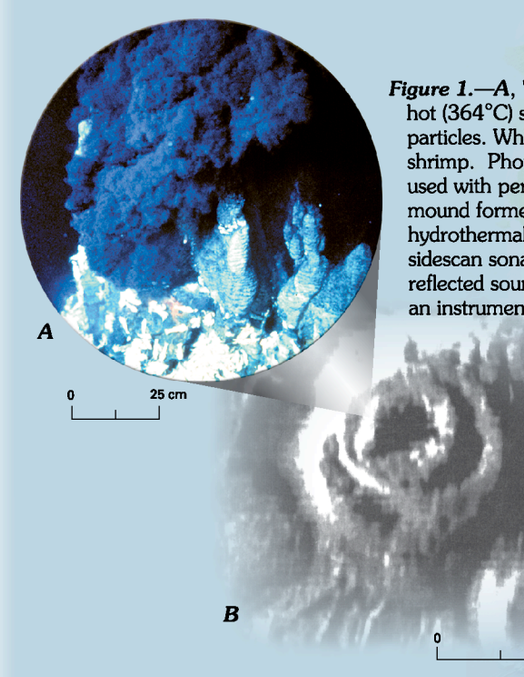

Figure 1.—*A*, "Black Smoker" (hydrothermal vent) jetting hot (364°C) seawater darkened by tiny metal-sulfide particles. White objects clustered on the vent chimney are shrimp. Photograph by Peter Rona (Rutgers University), used with permission. *B*, Doughnut-shaped, multi-ringed mound formed by thousands of years of deposits from hydrothermal activity like that shown in *A*. Image is from sidescan sonar, an important technique that uses reflected sound to "illuminate" features on either side of an instrument package towed near the sea floor. This mound, from the "TAG" hydrothermal field, is the largest discovered to date; other known similar hydrothermal features are much smaller and have been documented only by scientists in deep-diving submersibles (compare the different scale bars of the two images). Image from Marty Kleinrock (Vanderbilt University). Used with permission of American Geophysical Union.

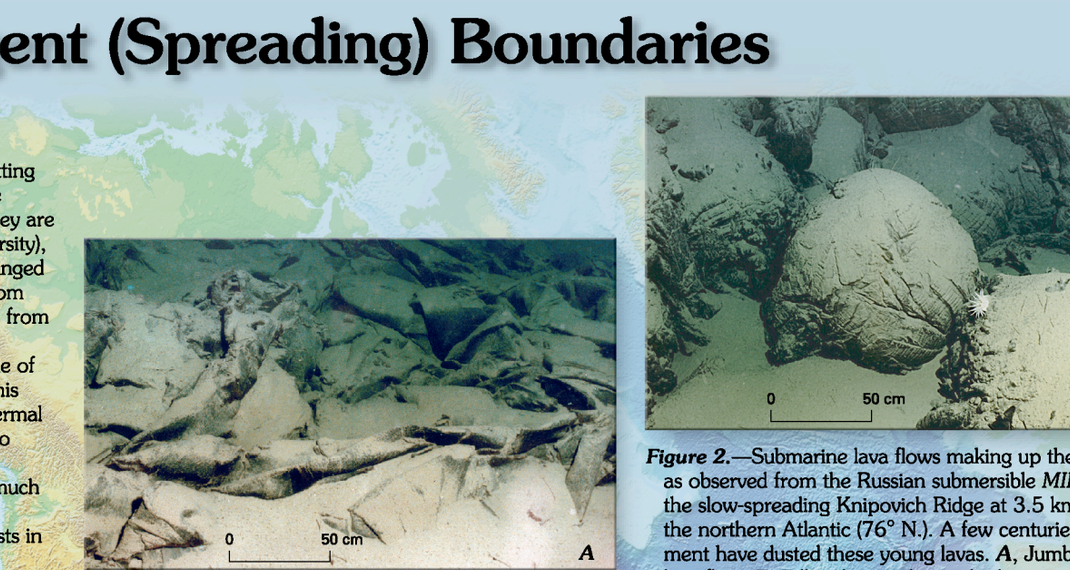

Figure 2.—Submarine lava flows making up the sea floor, as observed from the Russian submersible *MIR* exploring the slow-spreading Knipovich Ridge at 3.5 km depth in the northern Atlantic (76° N.). A few centuries of sediment have dusted these young lavas. *A*, Jumbled sheet lava flow. *B*, Pillow lava with attached sea anemone (white). Both photographs from Peter Vogt.

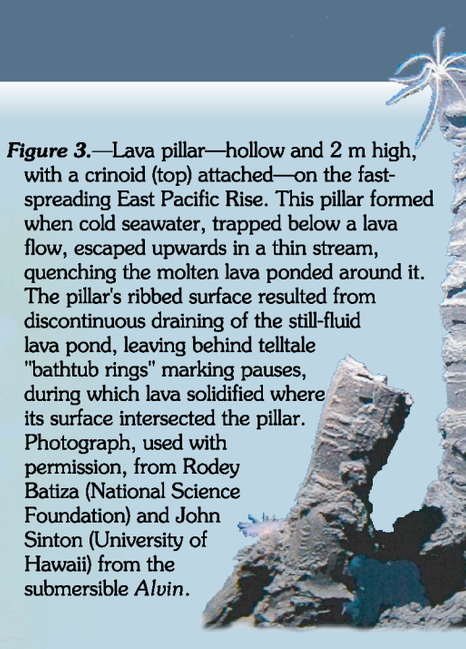

Figure 3.—Lava pillar—hollow and 2 m high, with a crinoid (top) attached—on the fast-spreading East Pacific Rise. This pillar formed when cold seawater, trapped below a lava flow, escaped upwards in a thin stream, quenching the molten lava ponded around it. The pillar's ribbed surface resulted from discontinuous draining of the still-fluid lava pond, leaving behind telltale "bathtub rings" marking pauses, during which lava solidified where its surface intersected the pillar. Photograph, used with permission, from Rodey Batiza (National Science Foundation) and John Sinton (University of Hawaii) from the submersible *Alvin*.

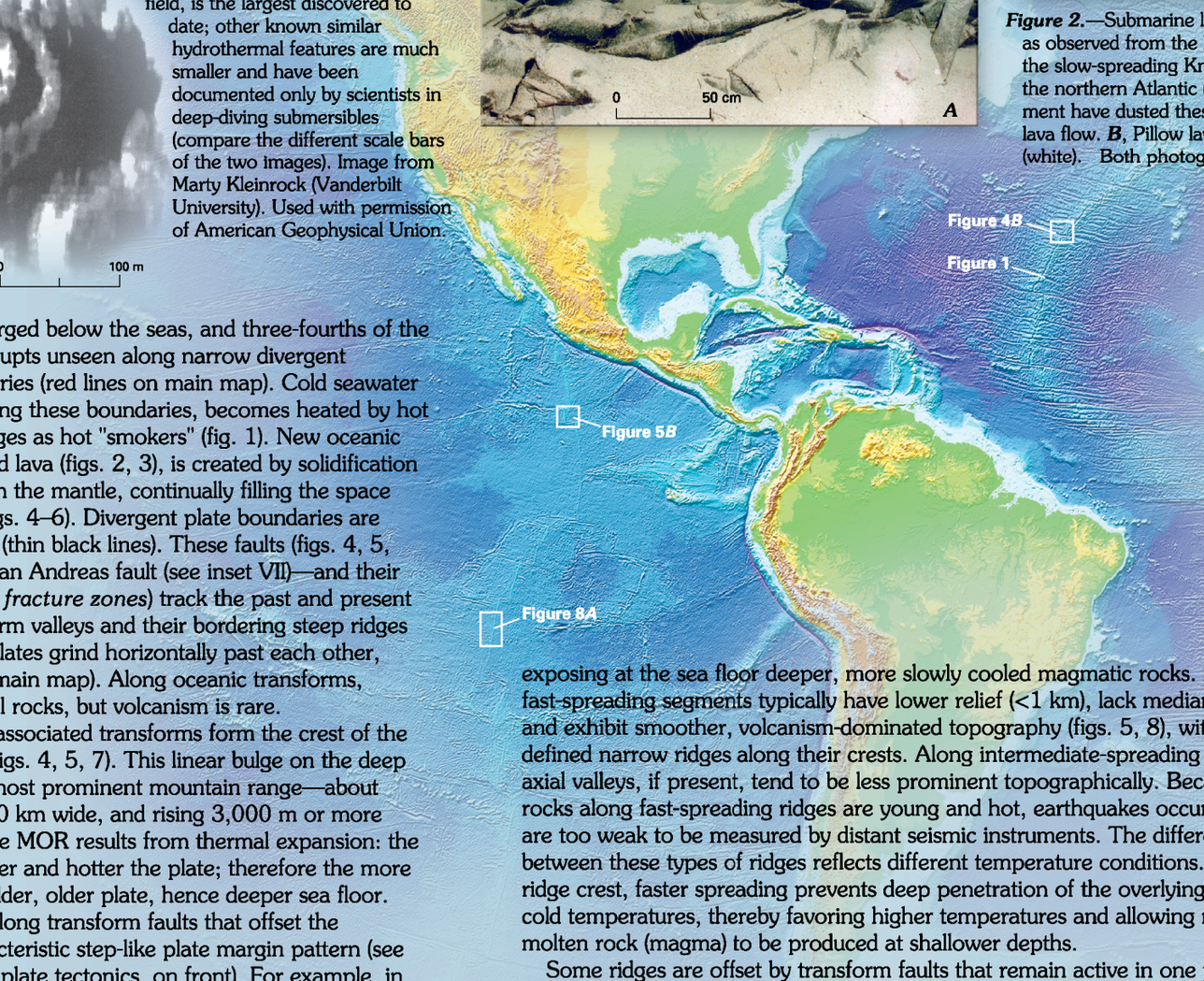

Most plate boundaries lie submerged below the seas, and three-fourths of the world's lava (average ~4 km³/yr) erupts unseen along narrow divergent (*spreading* or *rifting*) plate boundaries (red lines on main map). Cold seawater circulates down through cracks lacing these boundaries, becomes heated by hot volcanic rocks, and locally re-emerges as hot "smokers" (fig. 1). New oceanic crust, commonly capped by erupted lava (figs. 2, 3), is created by solidification of molten rock (*magma*) rising from the mantle, continually filling the space created by the separating plates (figs. 4–6). Divergent plate boundaries are offset by oceanic *transform faults* (thin black lines). These faults (figs. 4, 5, 7)—submarine equivalents of the San Andreas fault (see inset VII)—and their inactive extensions (together called *fracture zones*) track the past and present directions of plate motion. Transform valleys and their bordering steep ridges mark plate boundaries where the plates grind horizontally past each other, accompanied by earthquakes (see main map). Along oceanic transforms, faulting locally exposes deep crustal rocks, but volcanism is rare.

Divergent plate boundaries and associated transforms form the crest of the global Mid-Oceanic Ridge (MOR) (figs. 4, 5, 7). This linear bulge on the deep ocean floor is Earth's longest and most prominent mountain range—about 65,000 km long, as much as 1,000 km wide, and rising 3,000 m or more above the flanking deep basins. The MOR results from thermal expansion: the closer to the ridge crest, the younger and hotter the plate; therefore the more expanded and higher above the colder, older plate, hence deeper sea floor. *Relief* along the MOR is greatest along transform faults that offset the spreading ridge, forming the characteristic step-like plate margin pattern (see main map and interpretive map of plate tectonics, on front). For example, in the equatorial Atlantic Ocean, the Romanche Fracture Zone—7,728 m at its deepest—is even deeper than several subduction zone trenches (see inset II). Spreading (total opening) rates range from about 150 mm/yr along the East Pacific Rise (figs. 5, 8) to less than 10 mm/yr along the Arctic extension of the Mid-Atlantic Ridge. Scientists generally consider rates of less than 60 mm/yr as "slow" and rates greater than 90 mm/yr as "fast." Spreading "half rates" are not always the same on opposing sides of the plate boundary, however. Note how the present boundary is closer to the eastern than to the western lines of equal age (0.78 Ma) in the southern part of figure 7.

Local relief and structures along the ridge crests range widely, depending on spreading rate. High relief (1–2 km) and a prominent axial rift valley are characteristic of slow-spreading MOR segments, where a combination of tensional faulting and volcanism produces a complex structure (fig. 4*A*), locally exposing at the sea floor deeper, more slowly cooled magmatic rocks. In contrast, fast-spreading segments typically have lower relief (<1 km), lack median valleys, and exhibit smoother, volcanism-dominated topography (figs. 5, 8), with well-defined narrow ridges along their crests. Along intermediate-spreading ridges, axial valleys, if present, tend to be less prominent topographically. Because the rocks along fast-spreading ridges are young and hot, earthquakes occurring there are too weak to be measured by distant seismic instruments. The difference between these types of ridges reflects different temperature conditions. At the ridge crest, faster spreading prevents deep penetration of the overlying ocean's cold temperatures, thereby favoring higher temperatures and allowing more molten rock (magma) to be produced at shallower depths.

Some ridges are offset by transform faults that remain active in one place for many millions of years. Other ridge offsets, especially along fast-spreading boundaries (fig. 5*B*), are active for much shorter times and may move along some ridges that lengthen (*propagate*) during spreading. MOR spreading boundaries are not always perpendicular to the nearest transform. Oblique (non-perpendicular) spreading (for example, north of 30.5° N. in fig. 4*B*) is most common at slow-spreading ridges. Some rifts may even overlap along fast-spreading boundaries (fig. 5*B*).

Luckily for scientists, the oceanic crust operates like a giant "tape recorder" that remembers its creation and thus the rates at which its plates separated over time. As new oceanic crust forms along the MOR axis, it cools and becomes magnetized, locking in Earth's magnetic field at the time. Most of this magnetization resides in tiny *magnetite* crystals "frozen" in the erupted lava as it solidifies into rock. Occasional reversals of Earth's magnetic field are recorded by the oceanic crust as small but measurable, ridge-parallel stripe-like magnetic anomalies (*magnetic striping*). Magnetic-anomaly maps made by ships or airplanes can be used to calculate the magnetization of the crust (fig. 7). Because the times of magnetic reversals have been independently dated, the stripe-like pattern of normally and reversely magnetized crust allows the calculation of past rates of sea-floor spreading. From these data, and traces of transform faults, past plate motions can be reconstructed and continents reassembled!

The "embryo" of a future midocean ridge segment begins to take shape when continental crust starts to split apart along active rift zones, as in east Africa. There, geologically young volcanoes (Mt. Kilimanjaro), basins formed by down-dropped crustal blocks (Lake Tanganyika), and earthquake activity all foreshadow a future oceanic ridge segment between the Nubia and Somalia plates. With continued continental rifting, a new ocean basin such as the Red Sea is born. Over the long span of geologic time, new rifts break through some plates, other plate boundaries become inactive (see interpretive map), and existing plate boundaries migrate over the deeper mantle in an ever-shifting mosaic of plates. Oceans eventually die, as oceanic crust is recycled by subduction and continents collide, leaving only new mountain chains as evidence of their passing (see inset III).

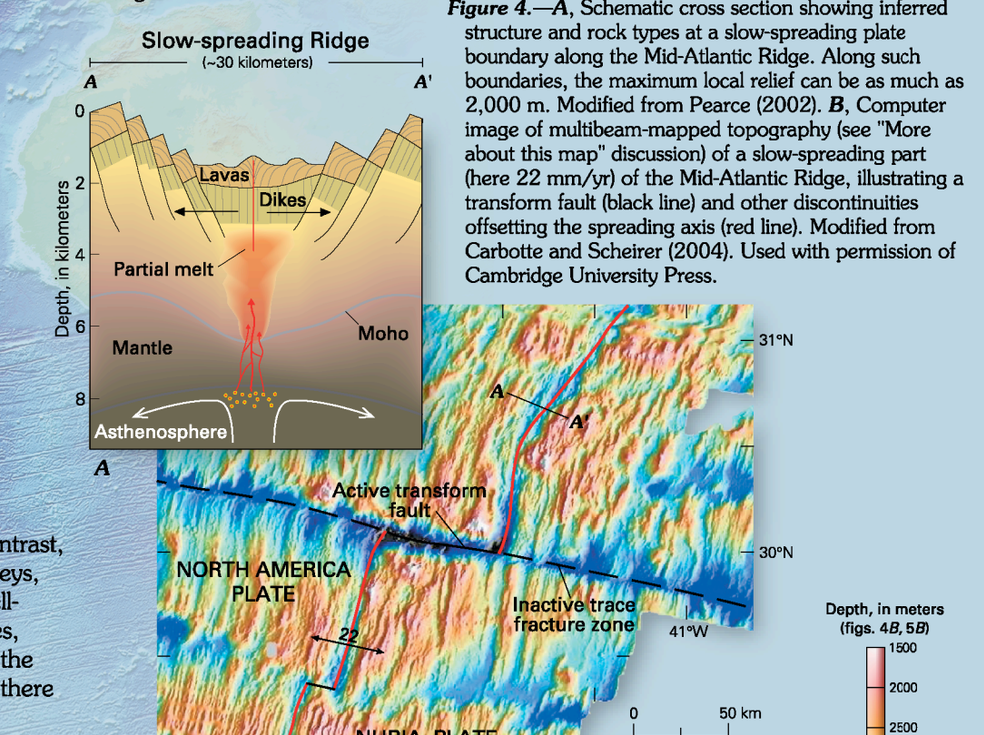

Figure 4.—*A*, Schematic cross section showing inferred structure and rock types at a slow-spreading plate boundary along the Mid-Atlantic Ridge. Along such boundaries, the maximum local relief can be as much as 2,000 m. Modified from Pearce (2002). *B*, Computer image of multibeam-mapped topography (see "More about this map" discussion) of a slow-spreading part (here 22 mm/yr) of the Mid-Atlantic Ridge, illustrating a transform fault (black line) and other discontinuities offsetting the spreading axis (red line). Modified from Carbotte and Scheirer (2004). Used with permission of Cambridge University Press.

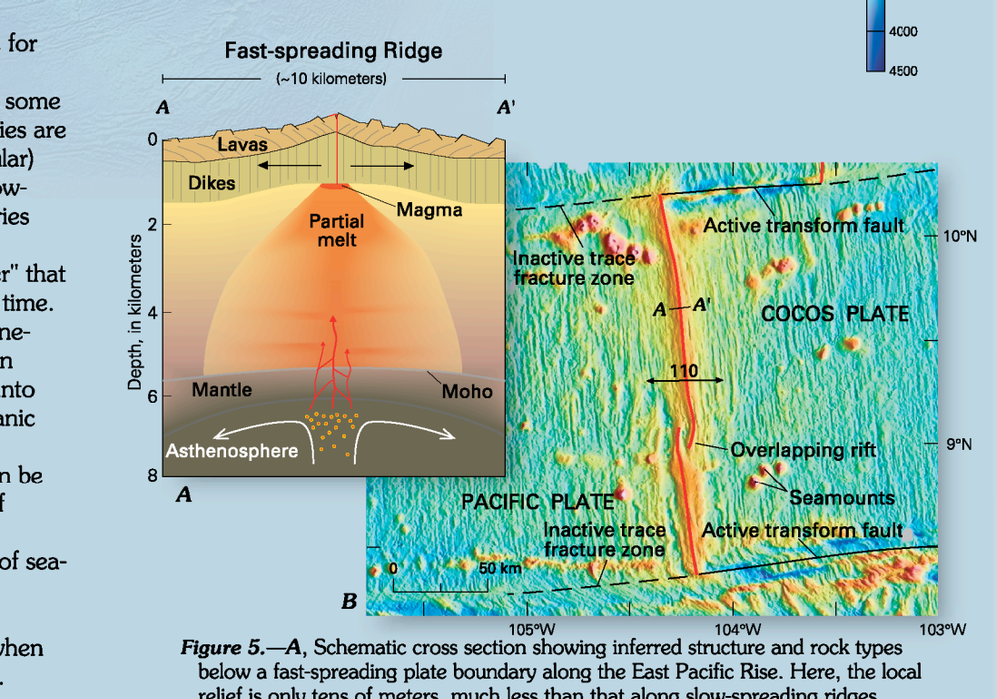

Figure 5.—*A*, Schematic cross section showing inferred structure and rock types below a fast-spreading plate boundary along the East Pacific Rise. Here, the local relief is only tens of meters, much less than that along slow-spreading ridges (compare with fig. 4*A*). Modified from Pearce (2002). *B*, Computer image of multibeam-mapped topography of a fast-spreading part (here 110 mm/yr) of the East Pacific Rise, showing two transform faults and an overlapping southward-propagating rift (too small to show on the main map). Modified from Carbotte and Scheirer (2004). Used with permission of Cambridge University Press.

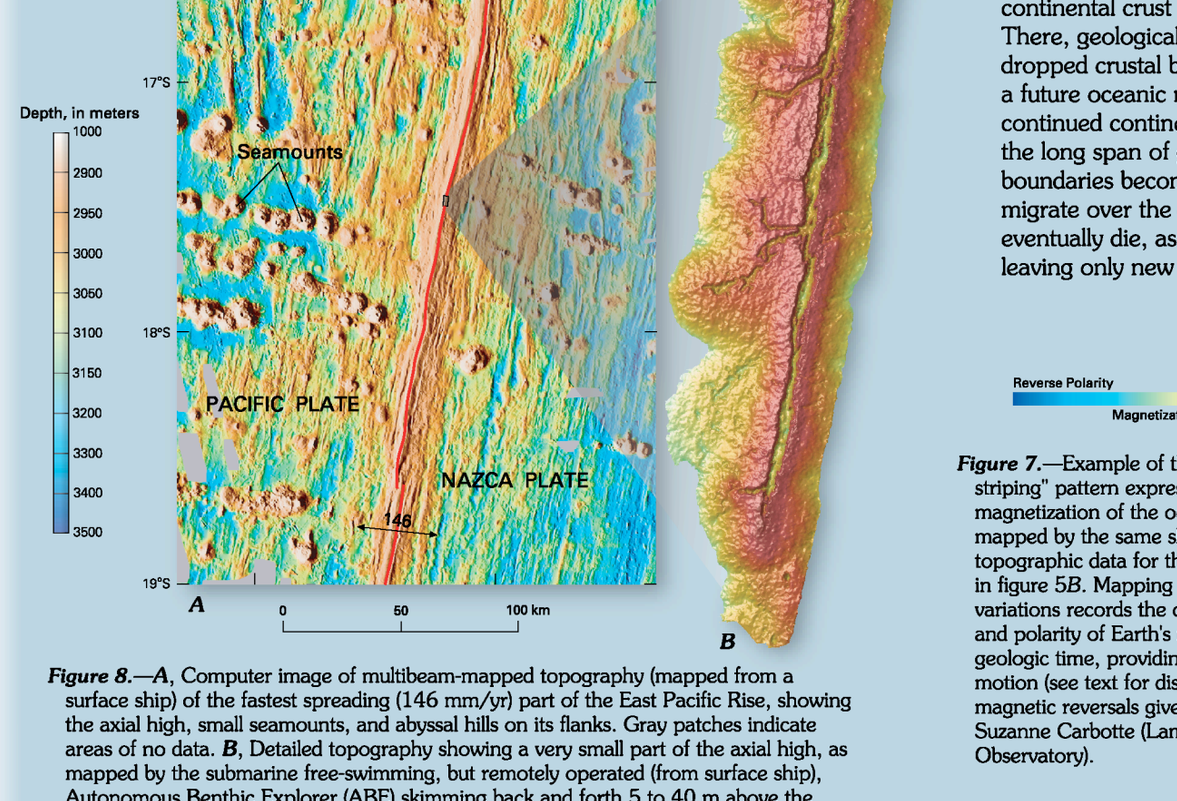

Figure 8.—*A*, Computer image of multibeam-mapped topography (mapped from a surface ship) of the fastest spreading (146 mm/yr) part of the East Pacific Rise, showing the axial high, small seamounts, and abyssal hills on its flanks. Gray patches indicate areas of no data. *B*, Detailed topography showing a very small part of the axial high, as mapped by the submarine free-swimming, but remotely operated (from surface ship), Autonomous Benthic Explorer (ABE) skimming back and forth 5 to 40 m above the deep sea floor. Note the narrow (50-m-wide), 10-m-deep central fissure valley, the remains of a long lava lake that drained through channels feeding lobes to the west. Images from Marie-Hélène Cormier (Lamont-Doherty Earth Observatory).

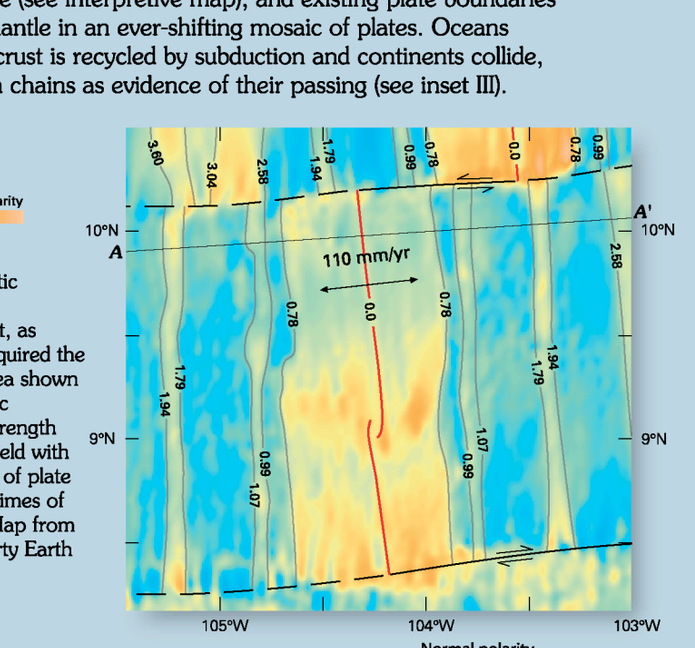

Figure 7.—Example of the "magnetic striping" pattern expressing the magnetization of the oceanic crust, as mapped by the same ship that acquired the topographic data for the same area shown in figure 5*B*. Mapping of magnetic variations records the changing strength and polarity of Earth's magnetic field with geologic time, providing a history of plate motion (see text for discussion). Times of magnetic reversals given in Ma. Map from Suzanne Carbotte (Lamont-Doherty Earth Observatory).

Figure 6.—Iceland is a "hotspot" (see interpretive map of plate tectonics, on front) and one of the few places where the global Mid-Oceanic Ridge system emerges above sea level. This southeast-looking aerial view shows Krafla Volcano, Iceland, erupting on September 8, 1977. Lava fountains spout from a 900-m-long fissure—part of the spreading Mid-Atlantic Ridge—and feed lava flows advancing over snow-covered ground. During this intermittent eruption, lasting from 1975 to 1984, the fissure widened by 8 m. Photograph by Sigurdur Thorarinsson.

MORE ABOUT THIS MAP

INTRODUCTION

Our Earth is a dynamic planet, as clearly illustrated on the main map (on front) by its topography, over 1,500 volcanoes, 44,000 earthquakes, and 170 impact craters. These features largely reflect the movements of Earth's major tectonic plates and many smaller plates or fragments of plates (including *microplates*). Volcanic eruptions and earthquakes are awe-inspiring displays of the powerful forces of nature and can be extraordinarily destructive. On average, about 60 of Earth's 550 historically active volcanoes are in eruption each year. In 2004 alone, over 160 earthquakes were magnitude 6 or above, some of which caused casualties and substantial damage.

THE DYNAMIC EARTH

As the main map shows, earthquakes and volcanoes are not randomly scattered over Earth's surface. Instead, most are concentrated along certain continental edges, along island chains, or along oceanic ridge crests. Although geologists have long known this, it has been only in the past 40 years that a concept has emerged to satisfactorily link these observations. This unifying concept, called *plate tectonics* (see Kious and Tilling, 1996), is now widely accepted and has revolutionized the earth sciences. Table 4 in the online version of this map (http://www.minerals.si.edu/minsci/tdpmap) lists some notable milestones and pioneers in the development of the plate tectonics theory.

Earth's outermost layer (the relatively stiff and rocky *lithosphere*) is a mosaic of large tectonic plates that move relative to one another at speeds measured in tens of millimeters per year—or about the same rate as our fingernails grow. Plates are cold, dense, and strong enough to resist most large deformation. They average about 80 km thick, but are generally thicker under continents than under oceans. Plates are composed of Earth's relatively thin surface rind (the *crust*) and the topmost 75 km of its 2,900-km-thick *mantle*. Over 50 separate plates are recognized by some specialists (for example, Bird, 2003), but the 15 that we name cover more than 95 percent of Earth's surface.

Plates move on a viscous, slowly flowing layer of hotter, softer mantle (the *asthenosphere*). Plate movement represents the top of a large-scale circulation system (*convection*)—driven by Earth's escaping heat—that extends deep into the mantle. Mantle flow is like the sluggish movement in a pot of thick soup boiling on a stove. Such flow transports the plates horizontally on Earth's surface. Where plates grind against each other, stresses can build up and be relieved intermittently when rocks break or slide along *faults*, causing earthquakes. Near some plate boundaries, molten rock (*magma*) can rise to the surface from as deep as many tens of kilometers and erupt to form volcanoes. Some plate boundaries cannot be narrowly defined, but instead are diffuse, encompassing broad areas (see interpretive map of plate tectonics, on front).

Most deformation associated with plate movements is concentrated in the boundary zones between shifting plates, explaining why so many earthquakes and volcanoes are found along or near plate boundaries. Nevertheless, active volcanism and large earthquakes also can occur in plate interiors, which are not immune from plate tectonic forces.

FEATURES OF THE MAP

Topography

Earth's topographic features are largely the expression of plate tectonics, modified by erosion. In the oceans, however, scattering of light in seawater prevents "seeing" most of the sea floor from aircraft or orbiting satellites. Radar waves, like light waves, also cannot penetrate deep into seawater, but they have been used successfully to map the ocean surface from satellites. This mapping technique (*satellite radar altimetry*) involves the measurement of small undulations of the sea surface—tens of kilometers across but only a few centimeters to meters in height—produced by slight differences in gravitational attraction of sea-floor mountains and valleys. These small variations in sea-surface height mimic, and are proportional to, the actual topographic features of the sea floor. Satellite-radar data provide global coverage, but resolve only the larger sea-floor features. Photographs or high-resolution topography are available for only a tiny fraction of 1 percent of the world's ocean floor. (See inset I for examples of sea-floor mapping at various scales.)

The sea-floor topography shown on the main map was produced from satellite-radar mapping of the sea surface, augmented in places by data obtained by ship-based acoustic (echo-sounding) techniques. Sea-floor topography is typically "visualized" as computer-generated, colored maps. In reality, however, the deep ocean floor is sunless, totally dark, unless artificially and briefly lit. Land-surface topography is obtained by using similar satellite technology, but here radar mapping from space gives a direct measure of surface features. Shading—as if the topographic images were illuminated by an artificial sun at 20° above the northwestern horizon—helps the visualization of features.

A Mercator map projection is used, both for its familiarity and for ease of transferring information from other Mercator projection maps. This projection exaggerates the relative size of high-latitude areas, and we have omitted coverage beyond 72° N. and 70° S. on the main map. Polar projections in lower corners (65°–90°) complete the coverage of the planet at the equatorial scale of the main map.

Earthquakes

Earthquakes are vibrational motions produced mostly by rupture of rock along faults. The most common measure of earthquake "size," based on the amount of seismic ground motion, is called *magnitude*. This concept was introduced in the mid-1930s by seismologist Charles F. Richter. He measured a seismic-wave characteristic called *amplitude* (the height of the peak seismic wave recorded by standard seismographs at a standard distance from the earthquake source). Because peak amplitudes vary over such an enormous range among earthquakes, the Richter scale is logarithmic: a magnitude-6 earthquake has 10 times the peak amplitude and releases about 30 times more energy than a magnitude-5 earthquake. A magnitude-3 earthquake is about the smallest that can be felt by humans, and the largest ever recorded was 9.5. In general, the larger the magnitude, the larger the rupture area and movement along the fault. Small-magnitude earthquakes occur much more frequently than large-magnitude earthquakes (see earthquake explanation on front).

Map locations of earthquakes (*epicenters*) are determined from the precise arrival times of seismic waves at global seismic stations, the known speeds of those waves, and the principle of triangulation. Our ability to locate earthquake epicenters has greatly improved during the last decade because of sensitive digital seismic instruments and improved data processing. On the main map, modern accurate epicenters show that most earthquakes are closely clustered along plate boundaries. The most demanding test of earthquake-location accuracy is along oceanic plate boundaries that are typically distant from seismic stations on land. Comparison of the new earthquake locations with the similarly improved mapping of oceanic plate boundaries shows that most of these earthquakes occur neatly along transform fault segments. In contrast, spreading ridge crests, linked by these transforms, generate few detectible earthquakes, because plates there are too thin and weak to allow large stresses to build.

A small number of intraplate earthquakes are shown (as hexagons) on the main map despite their pre-1900 dates or failure to meet the precise location criteria of the main data set. These—as shown by notable earthquakes nos. 1, 4, and 5 (table 3)—are important reminders that devastating earthquakes also occur, albeit rarely, far from active plate boundaries.

Volcanoes

Volcanoes are shown in four categories on the basis of their most recent known eruption in the past 10,000 years. Because repose intervals between eruptions can be thousands of years, and because the historical record in many parts of the world is only a few hundred years, we have made only minor graphical distinction between the map symbols for the first three categories. Thus, any one of them might erupt within our lifetimes. Remember, though, that most of Earth's volcanism occurs along the midocean ridge crests, where countless submarine eruptions take place each year—sight unseen—deep on the ocean floor.

Impact Craters

Discoveries during the past decade allow us to show 30 more impact craters than we did on the 1994 edition of the map (Simkin and others, 1994). Still, the evidence of other impact craters has been destroyed or hidden by post-impact geologic processes; the presently known craters simply serve as a reminder of this cataclysmic process, particularly early in the history of the Earth-Moon system (see inset VI and timeline).

Plate Motions

Divergent plate speeds, measured largely from separations of magnetic stripes at oceanic ridge crests, generally confirmed by global positioning system (GPS) data, and then integrated into plate motion models, are shown on the main map with white numerals. Convergent plate motions (stubby arrows with numerals) are calculated from the same model. Thin arrows in plate interiors show less accurate "absolute" plate motions (over the deeper mantle).

ACKNOWLEDGMENTS

This map is a joint product of the Volcano Hazards Program and the Earthquake Hazards Program of the U.S. Geological Survey, the Global Volcanism Program of the Smithsonian Institution, and the U.S. Naval Research Laboratory. Many institutions and individuals helped us in its preparation in important ways, most notably R.G. Bilham and E.R. Engdahl (University of Colorado); S.M. Carbotte (Lamont-Doherty Earth Observatory); D.C. DeMets (University of Wisconsin); J. Hasse (Naval Ice Center); M. Holzer (Chatham High School, N.J.); W.-Y. Jung (U.S. Naval Research Laboratory); J.R. Keith, J.E. Robinson, M.J. Rymer, S.P. Schilling, and D.W. Scholl (all U.S. Geological Survey); and S. Stein (Northwestern University). Additional valuable help has been provided by: S. Aramaki, M. Beddoe, C.R. Bentley, S. Bhardwaj, G.P. Bird, S.C. Cande, M. Collier, M.-H. Cormier, D.J. Fornari, B.M. French, C. Gaina, L. Gordon, R.G. Gordon, M.C. Guffanti, J.K. Hall, R.N. Hey, D.R. Hutchinson, M. Jakobsson, O.B. James, A.C. Johnston, M.C. Kleinrock, R.D. Larter, R.A. Livermore, J.F. Luhr, K. Marks, T.J. McCoy, W.J. Morgan, R.D. Müller, C.G. Newhall, E.A. Okal, G. Plafker, R.W. Purdey, W.E. Rankin, P.A. Rona, P. Rossi, C.R. Scotese, A.K. Shah, J.S. Shelton, L.G. Siebert, W.H.F. Smith, S.S. Sorensen, S. Steinthorsson, B. Taylor, W.R. Thatcher, E. Thurnau, and J.F. Vigil. We also express our appreciation to the many colleagues, geoscience teachers, and students who provided thoughtful comments and helpful advice on how to improve the previous editions (1989, 1994) of this map and text. For a comprehensive summary of the contributors to the preparation of this edition, see the online version at http://www.minerals.si.edu/minsci/tdpmap

II. Sea Floor Disappears as Plates Sink Along Deep Ocean Trenches

Subduction zones occur where a plate created by sea-floor spreading comes together or converges with another plate by sinking (or *subducting*) beneath it. A deep trench typically forms on the ocean floor where the subducting plate bends downward toward the deep mantle (figs. 1–3). More than 75 percent of all earthquakes occur in subduction zones, by slip between plates and rupture within descending plates (called *slabs*), forming inclined zones to depths as great as 690 km below the surface. Huge amounts of oceanic crust (~20 km³/yr, or ~3 km²/yr of sea-floor area) are consumed along trenches during subduction. As slabs sink deep into hotter mantle, they warm, lose most of their stored water, and eventually soften to a state incapable of producing either volcanoes or earthquakes.

Subduction earthquakes have caused untold damage throughout human history, killing over 400,000 people in the past 40 years alone. This figure includes the effects of large shallow earthquakes that displace the sea floor, generating high-speed ocean waves (called *tsunamis*) that can travel great distances, devastating coastal communities (see fig. 4 and table 3).

The process of volcano building begins with the initially cold slab descending into the hotter mantle, warming and dehydrating as the water it contains is "sweated out." These low-density fluids can then migrate upward, triggering partial melting of the hot, weak mantle above. Because this melted material (or *magma*) is less dense than the surrounding solid mantle, it rises buoyantly (or "floats"). Some of the magma accumulates in near-surface magma chambers, and some migrates to Earth's surface where it erupts and forms chains of volcanoes—called *island arcs* in oceans or *volcanic arcs* on land—that typically parallel the nearby trench (see schematic cross section, on front, and fig. 3).

Subduction-zone eruptions can be either explosive, producing airborne and ground-hugging fragmental deposits, or non-explosive, producing lava flows. Arc volcanoes built from both fragmental materials and lava flows are typically steep-sided cones called *stratovolcanoes* (fig. 5). Volcanic arcs contain nearly 80 percent of historically active land volcanoes, including those producing some of Earth's most destructive eruptions (see table 2). Some island arcs, such as those north of New Zealand, have localized plate divergence behind them (*back-arc spreading*) that resembles spreading at midocean divergent plate boundaries.

During subduction, sediments and crustal rocks on the upper part of the downgoing slab can be scraped off and added (or *accreted*) to the upper plate. The sinking plate can mechanically erode the bottom of the upper plate. Some of the eroded material also can be added to the bottom of the overriding plate at greater depth (*underplating*). When oceanic lithosphere sinks beneath a continent, mountains are formed by the combined processes of accretion, thickening (by squeezing), underplating, and volcanism. South America's lofty, 8,000-km-long Andes mountain chain formed by such processes, producing Earth's highest volcanoes (see table 2).

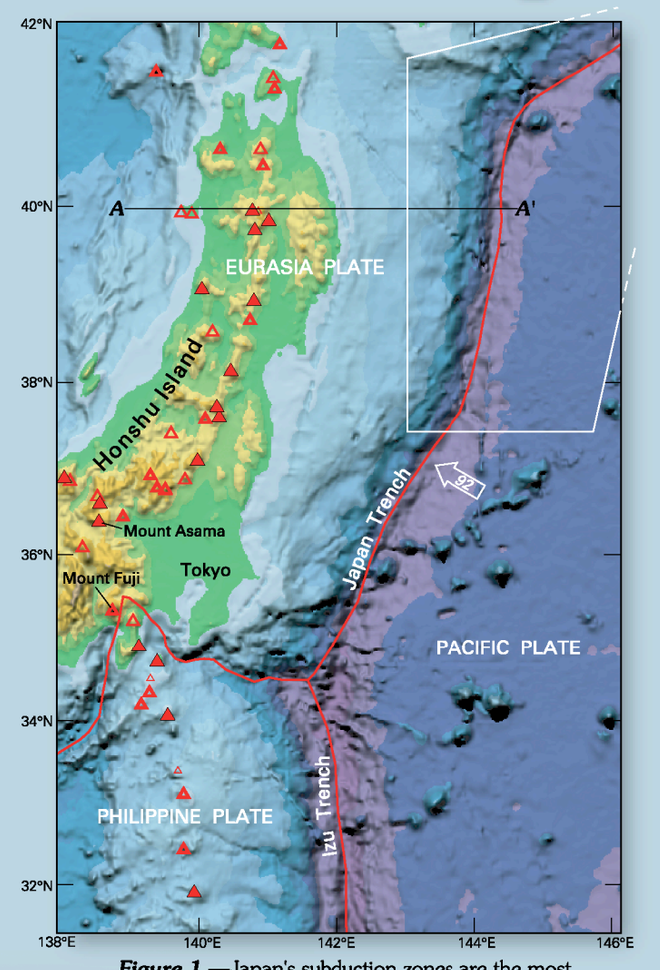

Figure 1.—Japan's subduction zones are the most closely studied in the world. Here, the Pacific plate sinks beneath Honshu Island, forming a deep trench, island-arc volcanoes, and a triple junction where it meets the Philippine plate. See main map for explanation of symbols. The approximate area of figure 2 is shown by the white outline.

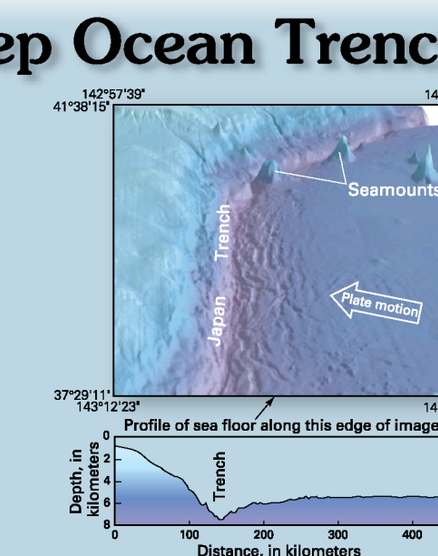

Figure 2.—Oblique view showing faulting of the sea floor where the Pacific plate bends and starts its descent, forming the Japan Trench, here over 7 km deep (see profile below image). Bending breaks the top of the slab, producing valleys and ridges that are roughly parallel to the trench. Image by Joel E. Robinson (USGS) from data collected by the Japan Hydrographic Department. Vertical exaggeration: image, ~10x; profile, ~20x.

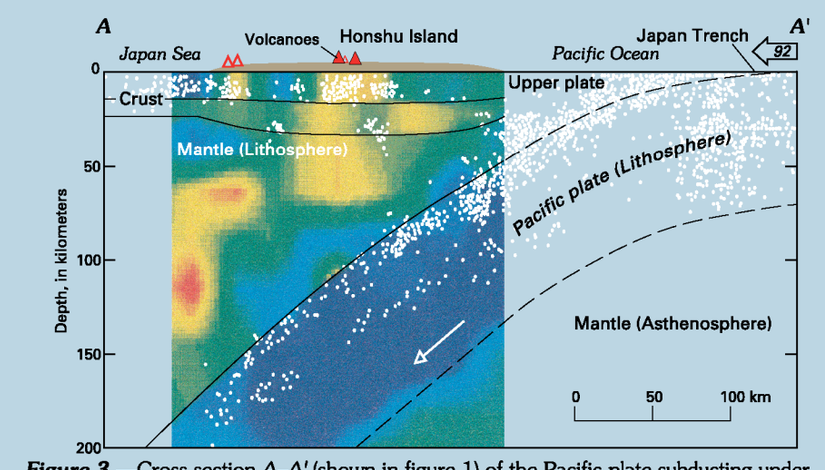

Figure 3.—Cross section *A–A'* (shown in figure 1) of the Pacific plate subducting under Japan. The color part of this figure is a computer image showing variations in seismic wave speeds. Seismic waves pass rapidly through the relatively cold Pacific plate (dark-blue areas) and pass more slowly through the surrounding, hotter mantle (light-blue to reddish areas). Earthquakes (white dots) occur within the cold, strong slab as well as within the overriding plate. Shallow crust under the active volcanoes is hot (yellow areas) and seismically active because rising magma weakens and promotes fracturing of the overlying rock. Modified from Zhao and others (1992). See main map for explanation of symbols.

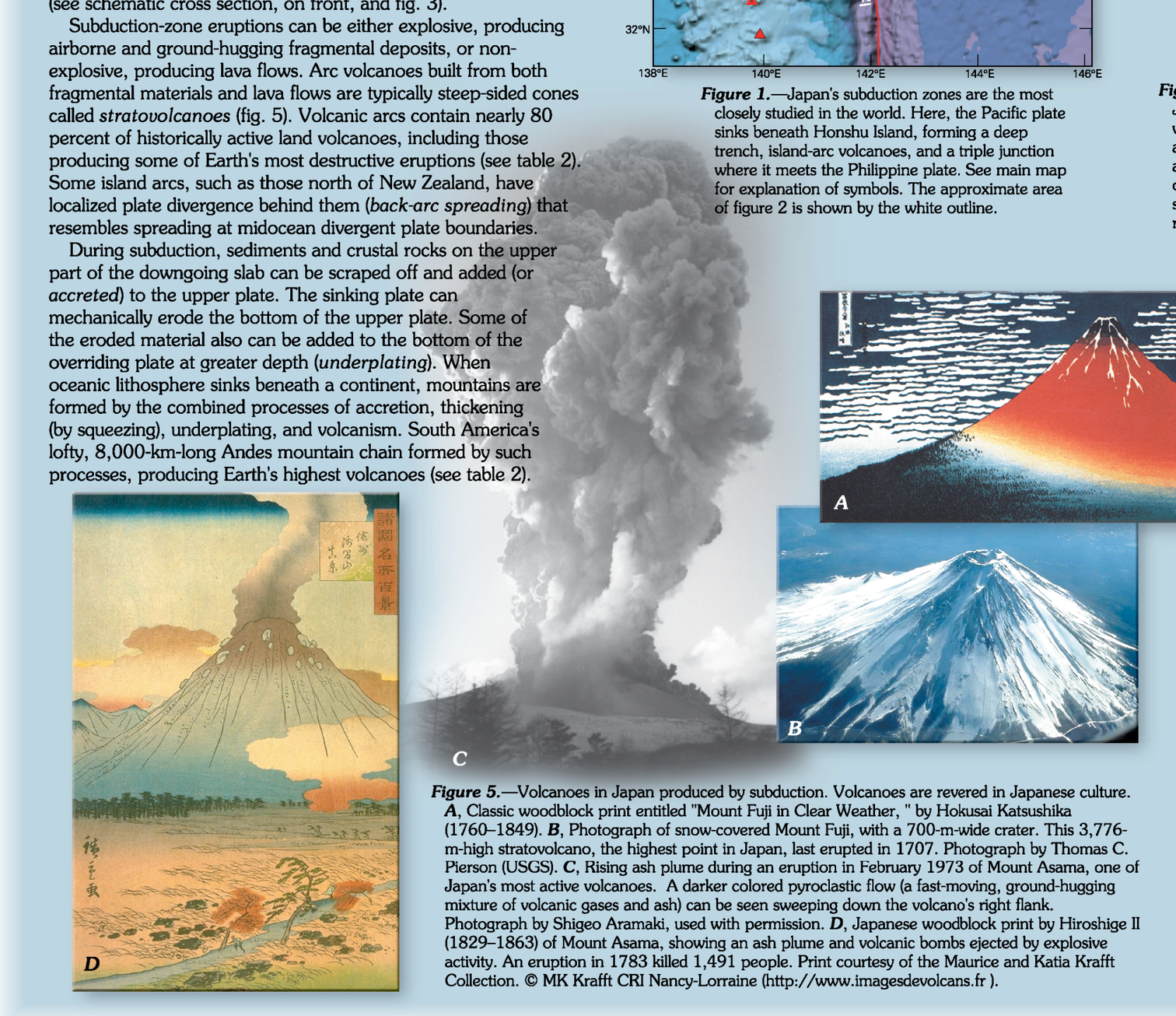

Figure 5.—Volcanoes in Japan produced by subduction. Volcanoes are revered in Japanese culture. *A*, Classic woodblock print entitled "Mount Fuji in Clear Weather, " by Hokusai Katsushika (1760–1849). *B*, Photograph of snow-covered Mount Fuji, with a 700-m-wide crater. This 3,776-m-high stratovolcano, the highest point in Japan, last erupted in 1707. Photograph by Thomas C. Pierson (USGS). *C*, Rising ash plume during an eruption in February 1973 of Mount Asama, one of Japan's most active volcanoes. A darker colored pyroclastic flow (a fast-moving, ground-hugging mixture of volcanic gases and ash) can be seen sweeping down the volcano's right flank. Photograph by Shigeo Aramaki, used with permission. *D*, Japanese woodblock print by Hiroshige II (1829–1863) of Mount Asama, showing an ash plume and volcanic bombs ejected by explosive activity. An eruption in 1783 killed 1,491 people. Print courtesy of the Maurice and Katia Krafft Collection. © MK Krafft CRI Nancy-Lorraine (http://www.imagesdevolcans.fr).

Figure 4.—Tsunami devastation in northern Sumatra, Indonesia, 2004. *A*, Satellite image of Lohknga (coastal Banda Aceh) before the December 26, 2004, earthquake that triggered deadly tsunamis (see table 3). *B*, Same scene 2 days after the tsunami struck; most buildings have been washed away, and the shoreline itself has been heavily eroded, in places entirely missing. QuickBird images acquired and processed by DigitalGlobe.

III. Colliding Continents Squeeze Up Mountain Ranges

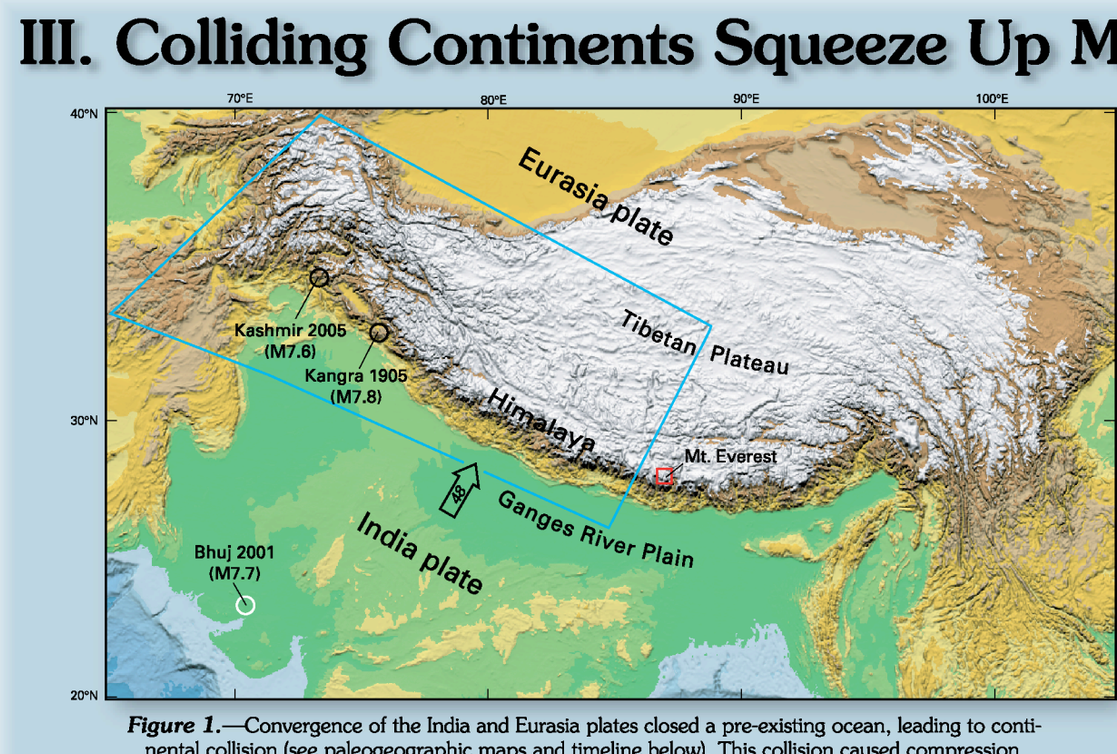

Figure 1.—Convergence of the India and Eurasia plates closed a pre-existing ocean, leading to continental collision (see paleogeographic maps and timeline below). This collision caused compression (squeezing) across a broad, diffuse boundary zone, producing Earth's highest land—the Himalaya and Tibetan Plateau. Compression is mostly taken up within the Himalaya-Tibetan region but extends far into the Eurasia plate. The approximate area of figure 2 is shown by the blue outline.

Figure 2.—View from space looking west showing (left to right): (1) the Ganges River Plain (blue area), (2) the white snow-and-cloud-covered Himalaya, with many peaks exceeding 7,300 m elevation, and (3) the Tibetan Plateau (brown, with blue lakes), at an average elevation of more than 4,880 m, higher than the Rocky Mountains. Space Shuttle image from NASA, no. STS41G–120–22.

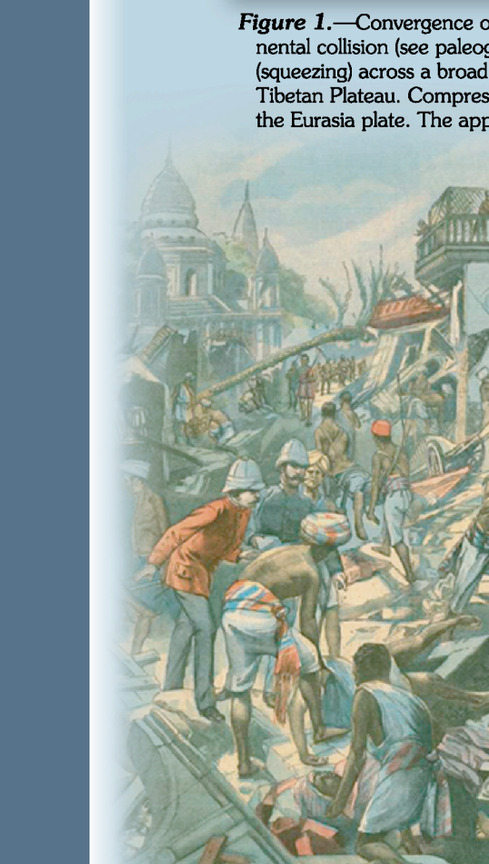

Figure 5.—1905 magazine print (from "Petit Parisien," "Supplément Littéraire Illustré," p. 144) showing rescue efforts after an M7.8 earthquake in the city of Kangra, India. Nearly 20,000 people perished, mostly in collapsed buildings and earthquake-triggered landslides. From the collection of Roger Bilham (University of Colorado).

Not all convergent plate boundaries involve *subduction* of oceanic lithosphere. When continental portions of converging plates collide, neither is subducted because both have low density and cannot easily sink deep into the denser mantle beneath. Such collision produces horizontal deformation (squeezing) and uplift of continental crust to build mountains and plateaus (figs. 1–4). "Continent-continent" collisions typically follow closure (by subduction) of a pre-existing ocean basin that formerly had separated the continents.

During collision, the crust of one plate shortens and thickens, and the adjacent plate thrusts under it, building high mountains such as the Himalaya, Alps, Caucasus, and Zagros. These regions of present-day mountain building experience frequent large and destructive shallow earthquakes (fig. 5). In some collision zones, such as those in Romania, Afghanistan, and Burma (Myanmar), earthquakes at depths greater than 60 km can occur in previously subducted oceanic lithosphere. Because of active convergence, low-density continental rocks become *sutured* together across the plate boundary, and are preserved as mountain belts in plate interiors (for example, Appalachians, Caledonides, and Urals), providing evidence of ancient, now inactive, collision zones. Unlike most subduction zones, continental collision zones produce little or no active volcanism.

The grandest of continental collision zones thrusts the India plate under the Eurasia plate, shortening and thickening the crust to produce Earth's highest mountains, the Himalaya (figs. 1–4). This deformation extends thousands of kilometers north of the Himalaya into the heart of the Eurasia plate (fig. 1), forming a *diffuse plate boundary zone* (see interpretive map of plate tectonics, on front). The deforming crust caught in the collision zone is squeezed and shoved sideways toward Southeast Asia—a process dubbed *escape tectonics*. In many collision zones, deformation is broadly distributed, highly complex, and cannot be characterized by a sharply defined plate boundary.

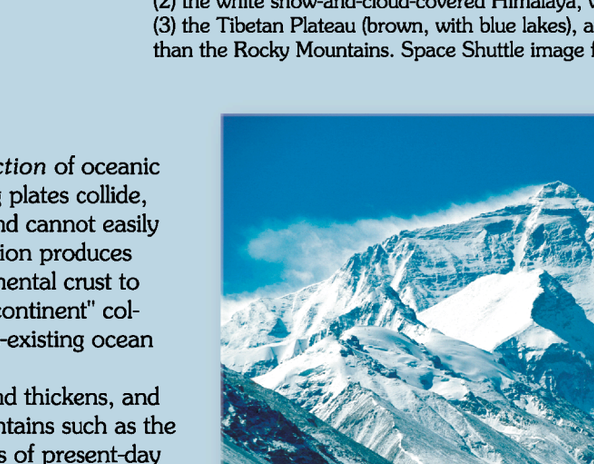

Figure 3.—At 8,848 m elevation, Mount Everest (*Chomolongma* in Tibetan) is the world's highest mountain. The peak is still rising a few millimeters per year as collision continues to occur. Marine fossils found in rocks high on Mount Everest attest to their large vertical uplift from the former sea floor. Photograph by Michael Searle (Oxford University), used with permission.

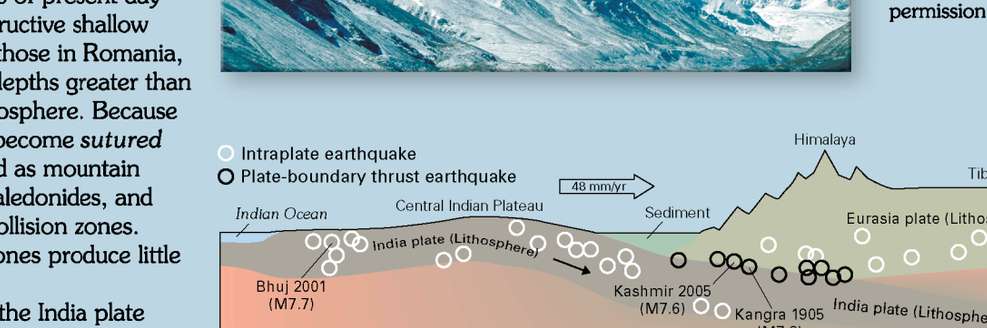

Figure 4.—Schematic diagram showing the India plate (brown) thrusting under the Eurasia plate (tan), effectively doubling the plate thickness under the Himalaya. Many destructive earthquakes occur in the foothills near the shallow thrust boundary between the two colliding plates, including the deadly M7.8 Kangra earthquake of 1905 and the devastating M7.6 Kashmir earthquake of 2005. The diagram also shows the bending by shortening of the India plate itself, which also causes earthquakes, such as the M7.7 Bhuj earthquake of 2001. Modified from Roger Bilham (University of Colorado).

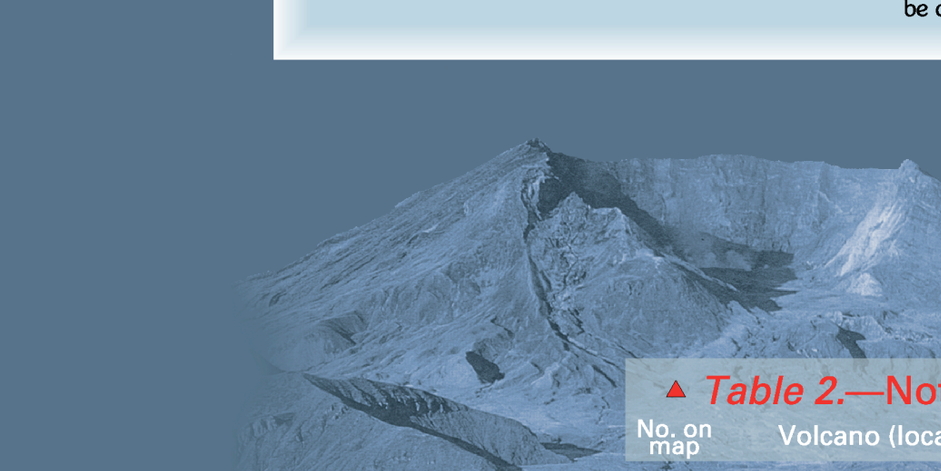

▲ *Table 2.*—Notable volcanic eruptions

No. on map	Volcano (location)	Date	Importance	Lat	Long
1	Yellowstone (Wyoming, U.S.A.)	2 Ma	Huge eruption (2,500 km³ of magma) blanketed western U.S. with ash (>2 cm in California, 1,500 km away; see inset V).	44.4° N.	110.7° W.
2	Santorini (Greece)	1640 B.C.	Bronze Age caldera-forming eruption influenced decline of Minoan civilization; tsunami may have inspired biblical flood legends.	36.4° N.	25.4° E.
3	Etna (Italy)	1500 B.C.	First historically documented eruption; Europe's largest volcano, Etna has been frequently active since.	37.7° N.	15.0° E.
4	Vesuvius (Italy)	A.D. 79	Pompeii and Herculaneum buried; earliest known written account for any eruption, by Pliny the Younger.	40.8° N.	14.4° E.
5	Taupo (New Zealand)	~180	16,000 km² (15 percent of North Island) devastated; only a tranquil caldera lake now marks the eruption site.	38.8° S.	176.0° E.
6	Rabaul (Papua New Guinea)	540±90	Explosive eruption formed caldera, later filled by the sea; regional volcano observatory established after 1937 eruption.	4.3° S.	152.2° E.
7	Ojos del Salado (Chile)	~700	World's highest active volcano, at 6,887 m; no known historical eruptions, but strong fumarolic activity.	27.1° S.	68.5° W.
8	Laki-Grímsvötn (Iceland)	1783	Enormous lava flows; livestock poisoned by volcanic fluorine and 10,000 Icelanders starve; cooled Europe's climate.	64.4° N.	17.3° W.
9	Unzen (Japan)	1792	Japan's deadliest eruption; collapse of dome produced debris avalanche and tsunami, killing 14,500.	32.8° N.	130.3° E.
10	Tambora (Indonesia)	1815	Largest historical explosive eruption, resulting in ~60,000 deaths and 1816's "year without summer" (June snow in New England!).	8.3° S.	118.0° E.
11	Krakatau (Indonesia)	1883	Caldera collapse; 40-m-high tsunamis kill >34,000; explosions heard >4,500 km away; vivid sunsets.	6.1° S.	105.4° E.
12	Montagne Pelée (West Indies)	1902	High-speed, incandescent pyroclastic flows kill 28,000 in minutes; response launched modern volcanology.	14.8° N.	61.1° W.
13	Santa María (Guatemala)	1902	5,000 killed when volcano erupts after long repose; growth of lava dome began 20 years later and continues to date.	14.8° N.	91.6° W.
14	Novarupta-Katmai (Alaska, U.S.A.)	1912	Largest 20th century eruption (including "Valley of Ten Thousand Smokes"); sound heard 1,200 km away.	58.3° N.	155.2° W.
15	Parícutin (Mexico)	1943	Volcano birth in cornfield witnessed by farmers; cinder cone grows to 336-m height in first year, to 424 m by 1952.	19.5° N.	102.3° W.
16	Surtsey (Iceland)	1963	New island formed by 4-year eruption, providing field laboratory for biologists to study arrival of flora and fauna to new land.	63.4° N.	20.3° W.
17	Tolbachik (Kamchatka)	1975	Eruption time and place accurately predicted (TV crews were on hand), in world's most volcanically active region.	55.8° N.	160.3° E.
18	Nyiragongo (Congo)	1977	Highly fluid flows from summit lava lake reached speeds of 60 km/hr; slower flows in 2002 engulfed center of Goma city.	1.5° S.	29.3° E.
19	Mount St. Helens (Washington, U.S.A.)	1980	Well-studied landslide showed that flank collapse can trigger explosive eruptions; such occurrences found to be common worldwide.	46.2° N.	122.2° W.
20	Kilauea (Hawaii, U.S.A.)	1983	Start of ongoing rift eruption, longest-running in Hawaii since A.D. 1400; has already created ~2.2 km² of new land.	19.4° N.	155.3° W.
21	Ruíz (Colombia)	1985	Small eruption melted icecap of 5,389-m-high volcano; resulting mudflows killed >22,000, in towns ≥40 km from crater.	4.9° N.	75.3° W.
22	Oshima (Japan)	1986	Highest historical lava fountains (>1,500 m); this island south of Tokyo has erupted more than 80 times since A.D. 605.	34.7° N.	139.4° E.
23	Redoubt (Alaska, U.S.A.)	1989	Jumbo jet's engines all fail in ash cloud, but two were restarted 1,500 m above mountains; $80 million damage to plane.	60.5° N.	152.8° W.
24	Pinatubo (Philippines)	1991	Evacuations save up to 20,000 lives; mudflow damage, some recurring long after eruption ended, leaves >200,000 homeless.	15.1° N.	120.4° E.
25	Juan de Fuca Ridge (off northwestern U.S.A.)	1993	First well-documented deep ocean eruption—world's most common type, but never witnessed—along divergent boundary (see inset I).	46.5° N.	129.6° W.

IV. Bedrock Ages Show Oceans Far Younger Than Continents

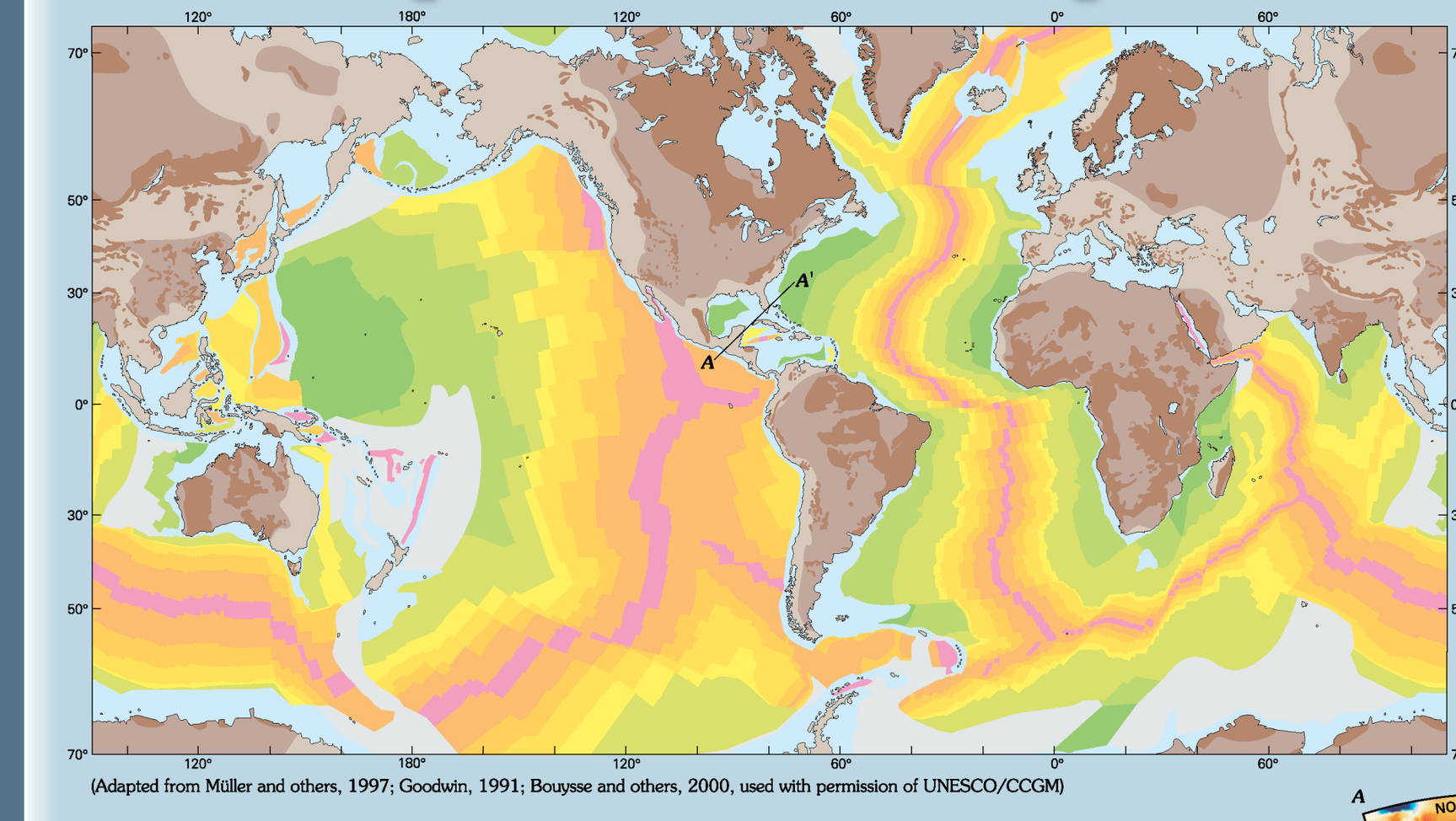

(Adapted from Müller and others, 1997; Goodwin, 1991; Bouysse and others, 2000, used with permission of UNESCO/CCGM)

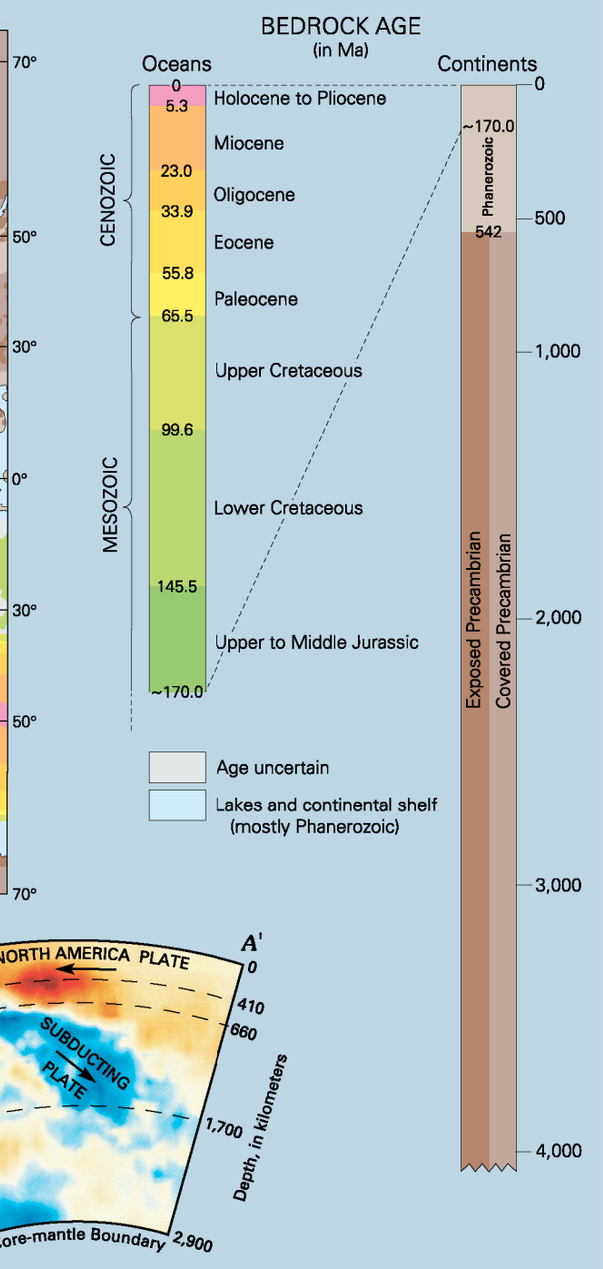

Newly created crust becomes progressively older, colder, and denser as it is carried away from divergent plate boundaries (generally the youngest oceanic rocks on the planet). Dense oceanic crust is ultimately recycled into the upper mantle at subduction zones. In contrast, less dense continental crust tends to "float," so that, over geologic time, much of it escapes this recycling process. Thus, as this map shows, the oldest bedrock of the sea floor (~170 Ma) is far younger than most continental bedrock. Precambrian rocks, older than 542 Ma, form the interiors of most continents and the cores of old continental mountain ranges, such as the Appalachians, Caledonides, and Urals. The yellow-green color boundary—between the Upper Cretaceous and Paleocene—represents oceanic crust that is 65 Ma, the age of the Chicxulub impact in eastern Mexico (see inset VI). This event caused massive extinctions. About 59 percent of the present-day oceanic crust has formed since Cretaceous time, when dinosaurs last roamed the land.

During the recycling process, subducting plates can remain largely undeformed to great depths before heating up, losing their physical identity, and ultimately being assimilated into the weak, slowly flowing mantle. An example is a profile (*A–A'*, center of map) across Central America (fig. 1), where the deep part of the subducting Cocos plate in the eastern Pacific Ocean projects beneath the Atlantic Ocean, offshore from North Carolina. Over geologic time, the positions of the continents and their associated subduction plate boundaries have shifted dramatically (compare Late Jurassic, K/T Boundary, and Last Glacial Maximum paleogeographic maps below). During the last 100 million years of eastward subduction under the Americas, the positions of the active plate boundaries have gradually shifted westward by more than 1,000 km.

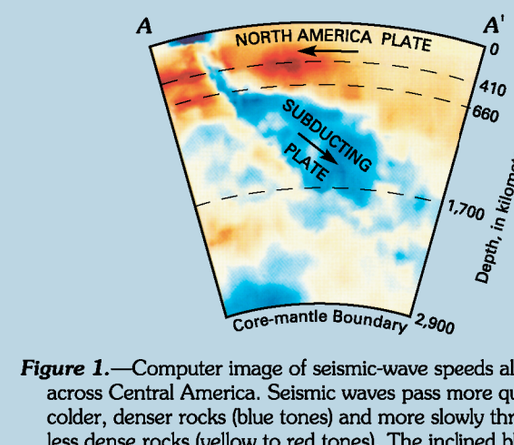

Figure 1.—Computer image of seismic-wave speeds along profile *A–A'* across Central America. Seismic waves pass more quickly through colder, denser rocks (blue tones) and more slowly through warmer, less dense rocks (yellow to red tones). The inclined blue-colored zone extending to 2,000 km depth is interpreted to represent the northeastward subduction of the Cocos plate and its predecessor beneath the southwestward-moving North America plate. Modified from Kárason and van der Hilst (2000). Used with permission of American Geophysical Union.

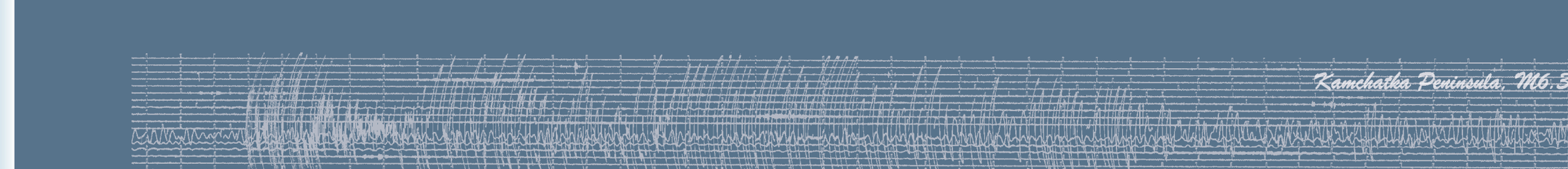

○ *Table 3.*—Notable earthquakes

[M=magnitude. Magnitudes listed here are selected from technical articles on these events and may differ from published catalog values]

No. on map	Earthquake (location)	Date	Importance	Lat	Long
1	Shanxi (eastern China)	1556	Deadliest earthquake on record with 830,000 reported killed. Near Xian, China's ancient capital.	35.5° N.	109.7° E.
2	Cascadia (Pacific Northwest, U.S.A.)	1700	M~9 shock; subsidence drowned local coastal forests and triggered tsunamis that damaged distant Japan.	47.6° N.	125.1° W.
3	Lisbon (Portugal)	1755	Offshore event that caused strong shaking, 6- to 15-m-high tsunamis, and a fire in Lisbon that killed ~60,000.	36.5° N.	11.3° W.
4	New Madrid (Missouri, U.S.A.)	1811–12	Three very large shocks over a 2-month period rang church bells near Philadelphia and cracked ice in the Chesapeake Bay.	36.0° N.	90.0° W.
5	Charleston (South Carolina, U.S.A.)	1886	Shaking felt from Bermuda to Minnesota; moderate to severe damage to masonry buildings in Charleston.	32.9° N.	80.1° W.
6	Nobi (Japan)	1891	Ground ruptures showed that movements along faults caused this M8 earthquake. First modern aftershock study.	35.4° N.	136.8° E.
7	Assam (northeastern India)	1897	M>8 earthquake in Himalaya collision belt; Earth's liquid iron core deduced from seismograms of the earthquake.	26.0° N.	91.0° E.
8	North Shikoku Basin (Japan)	1906	Earliest well-documented deep earthquake (340 km), showing that earthquakes can occur in Earth's deep mantle.	34.0° N.	137.0° E.
9	San Francisco (California, U.S.A.)	1906	M7.8 shock on San Andreas fault, and fire destroyed much of city (see inset VII). Stimulated earthquake science and elastic-rebound theory.	38.0° N.	123.0° W.
10	Messina (Italy)	1908	~85,000 dead from widespread effects of ground shaking, slope failures, fire, and a tsunami in the Strait of Messina.	38.0° N.	15.5° E.
11	Zagreb (Croatia)	1909	Mohorovičić discovered a jump in seismic-wave speeds, generally marking the crust-mantle boundary (the "Moho").	45.8° N.	15.9° E.
12	Gansu Province (China)	1920	M8.3–8.6 earthquake in the broad India-Eurasia collision belt. Widespread damage and ~200,000 deaths.	36.6° N.	105.3° E.
13	Kanto (south of Tokyo, Japan)	1923	M7.9 subduction shock killed 146,000 (99,000 in Tokyo), including losses from a tsunami and giant firestorm.	35.4° N.	139.1° E.
14	West Nelson (New Zealand)	1929	Earth's solid inner core, inside the liquid outer core, revealed in its seismic records (by Inge Lehmann in 1936).	41.8° S.	172.2° E.
15	Chillán (southern Chile)	1939	Occurred at 80-km depth within the subducting Nazca slab, causing 28,000 deaths; led to improved building codes in Chile.	36.2° S.	72.2° W.
16	Unimak Island (Alaska, U.S.A.)	1946	M8.5 shock triggered submarine landslide, generating tsunami with run-up to 31 m high on nearby Unimak Island and 18 m in Hawaii.	53.3° N.	162.9° W.
17	Offshore Kamchatka (Russia)	1952	Seismograms of this well-recorded M9 earthquake showed early evidence of slow, whole-earth vibrations.	52.8° N.	159.5° E.
18	Adreanof Islands (Alaska, U.S.A.)	1957	At M9.1, one of only five earthquakes in the magnitude 9 range, four in a 12-year period, since global recording began around 1895.	51.3° N.	175.8° W.
19	Valdivia (southern Chile)	1960	Largest earthquake (M9.5) yet recorded, confirming whole-earth vibrations; triggered a giant Pacific-wide tsunami.	38.2° S.	72.6° W.
20	Southern Alaska (U.S.A.)	1964	Second largest recorded earthquake (M9.2) caused extensive soil failure in Anchorage area and widespread tsunami damage.	61.1° N.	147.6° W.
21	Offshore northern Peru	1970	Within Nazca slab at 73-km depth, killing ~54,000, including 25,000 at Yungay, a town buried by an associated rock avalanche.	9.2° S.	78.8° W.
22	Tangshan (China)	1976	Devastated the city, causing the most fatalities for a 20th century earthquake—estimates range from 255,000 (official) to 655,000 (unofficial).	39.5° N.	117.9° E.
23	Northridge (California, U.S.A.)	1994	Rocked the Los Angeles basin; economic losses estimated to exceed $20 billion, a record for U.S. earthquakes.	34.2° N.	118.5° W.
24	Northwestern Bolivia	1994	Deepest large-magnitude earthquake (M8.3 at 636 km), with shaking felt to Canada; study of this event greatly refined Earth's structure.	13.8° S.	67.6° W.
25	Kobe (Japan)	1995	Major port city devastated: 5,500 dead, 310,000 homeless, and world record $150 billion in earthquake and fire losses.	34.6° N.	135.0° E.
26	Sumatra-Andaman (Indonesia)	2004	M9.0+ earthquake ruptures >1,000 km of subduction boundary; tsunamis kill a record ~230,000, some deaths as distant as Africa.	3.3° N.	96.0° E.

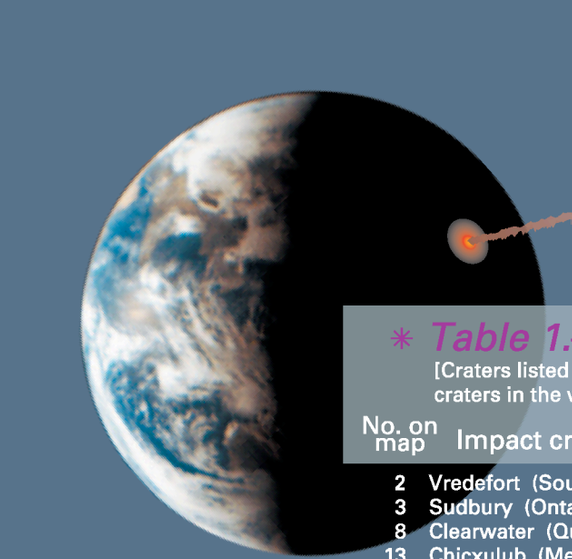

✳ *Table 1.*—Notable impact craters

[Craters listed here are from a longer list of consecutively numbered craters—arranged by age, oldest (no. 1) to youngest (no. 25)—selected from the 170 known craters in the world. See Web site version of this table for the complete listing of the 25 craters. Ma=million years ago. D=diameter]

No. on map	Impact crater (location)	Age (Ma)	Importance	Lat	Long
2	Vredefort (South Africa)	2023±4	Largest known structure (D=300 km); unique textural features indicate high-pressure shock impact.	27.0° S.	27.5° E.
3	Sudbury (Ontario, Canada)	1850±3	This large crater (D=200 km) is the only one with shock-melted body that hosts rich nickel-copper ore deposits.	46.6° N.	81.2° W.
8	Clearwater (Quebec, Canada)	290±20	Rare paired craters (D=26 and 36 km) formed by two close but separate bolides.	56.2° N.	74.5° W.
13	Chicxulub (Mexico)	64.98±0.05	Produced K/T (dinosaur) extinction event and global ejecta (with "fingerprint" iridium layer); see inset VI.	21.3° N.	89.5° W.
14	Montagnais (Nova Scotia, Canada)	50.50±0.76	First crater recognized at sea (buried on continental shelf); nearly all other known craters are on land.	42.9° N.	64.2° W.
15	Wanapitei (Ontario, Canada)	37.2±1.2	Younger, smaller crater inside Sudbury (no. 3); only known example of a second impact in the same place.	46.8° N.	80.8° W.
16	Popigai (Russia)	35.7±0.2	Detailed studies of this large (D=100 km) crater discovered diamonds produced by high-pressure shock waves.	71.7° N.	111.2° E.
17	Chesapeake Bay (Virginia, U.S.A.)	35.5±0.3	Largest crater in U.S.A. (D=85 km), buried by younger sediments, was discovered in 1980s by geophysical surveys.	37.3° N.	76.0° W.
23	Barringer (Meteor) (Arizona, U.S.A.)	0.049±0.003	"Textbook" crater (see inset VI)—the first recognized as caused by meteorite impact—was used in astronaut training.	35.0° N.	111.0° W.
25	Sikhote Alin (Russia)	0.000055	Large meteorite shower, seen by many in 1947, left >100 small craters and >8,000 meteorites over ~50 km² area.	46.1° N.	134.7° E.

V. Eruptions Through Plate Interiors Build Hotspot Volcanoes

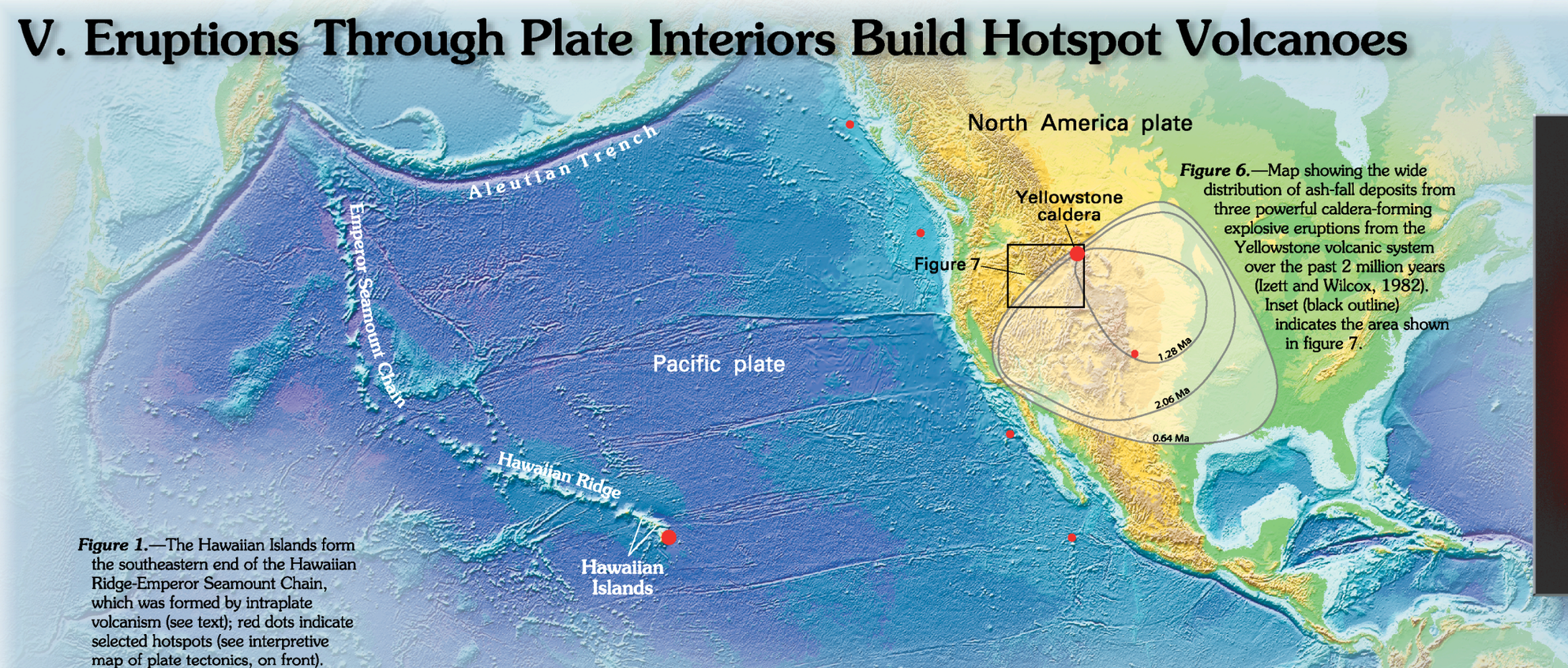

Figure 1.—The Hawaiian Islands form the southeastern end of the Hawaiian Ridge-Emperor Seamount Chain, which was formed by intraplate volcanism (see text); red dots indicate selected hotspots (see interpretive map of plate tectonics, on front).

Figure 6.—Map showing the wide distribution of ash-fall deposits from three powerful caldera-forming explosive eruptions from the Yellowstone volcanic system over the past 2 million years (Izett and Wilcox, 1982). Inset (black outline) indicates the area shown in figure 7.

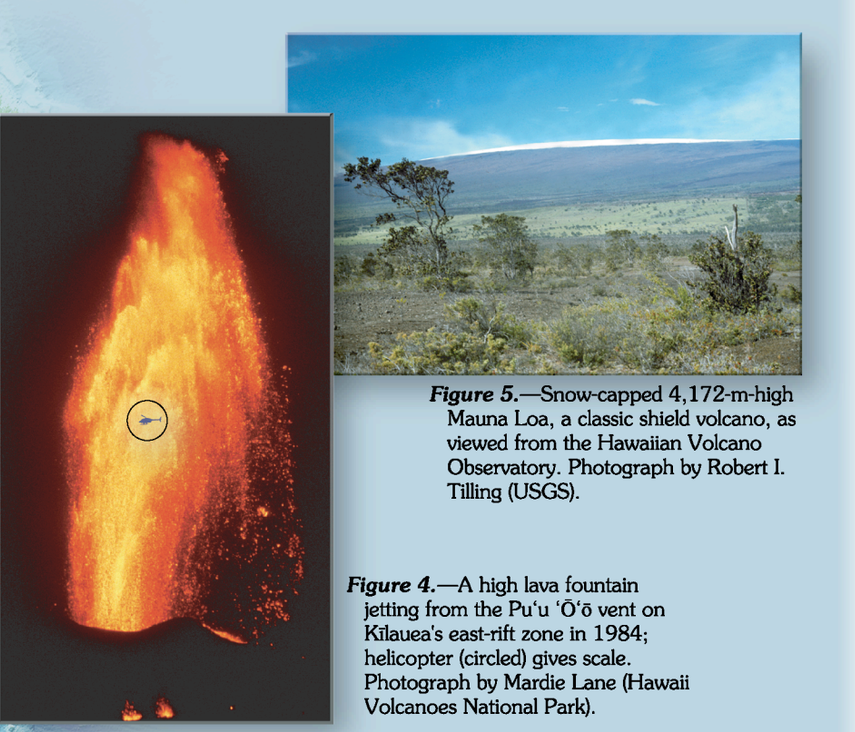

Figure 4.—A high lava fountain jetting from the Pu'u 'Ō'ō vent on Kīlauea's east-rift zone in 1984; helicopter (circled) gives scale. Photograph by Mardie Lane (Hawaii Volcanoes National Park).

Figure 5.—Snow-capped 4,172-m-high Mauna Loa, a classic shield volcano, as viewed from the Hawaiian Volcano Observatory. Photograph by Robert I. Tilling (USGS).

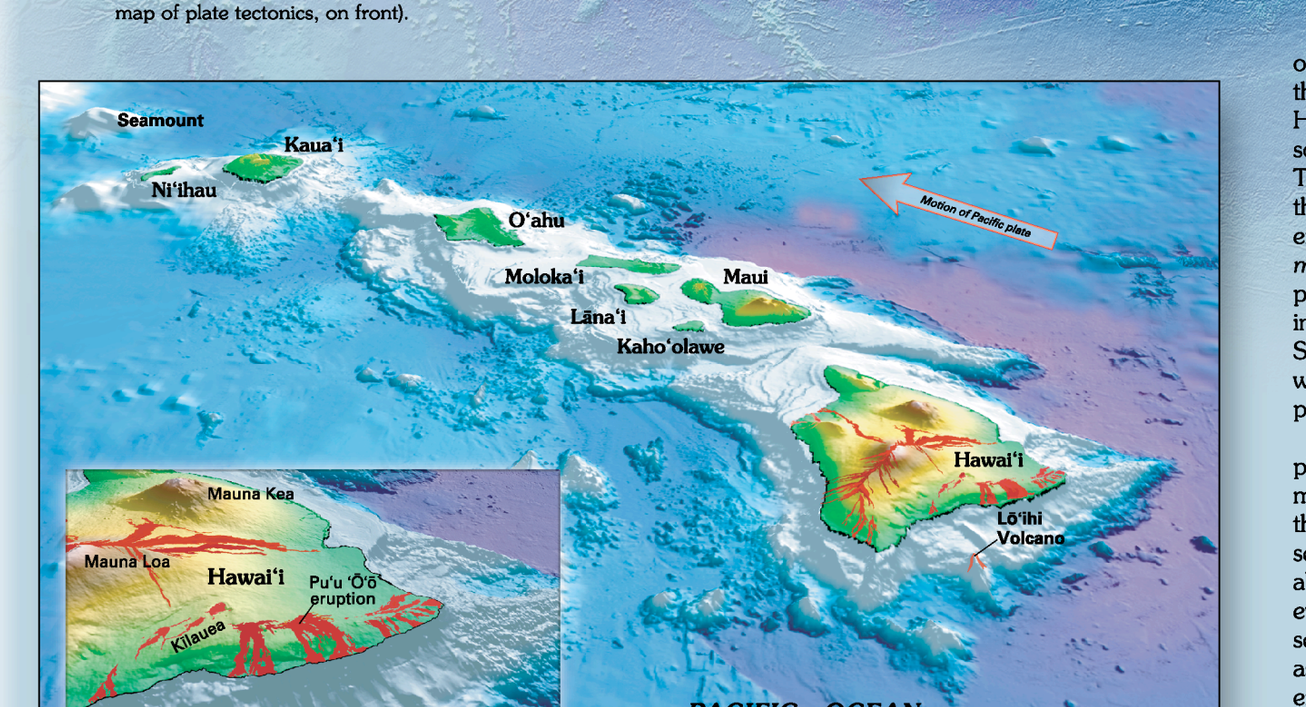

Figure 2.—Oblique view of the principal Hawaiian Islands and (the still submarine) Lō'ihi Volcano. Inset gives a closer view of three of the five volcanoes that form the Island of Hawai'i (historical lava flows are shown in red). The longest duration historical eruption on Kīlauea's east-rift zone at Pu'u 'Ō'ō (inset), which began in January 1983, continues unabated (as of spring 2006). View prepared by Joel E. Robinson (USGS).

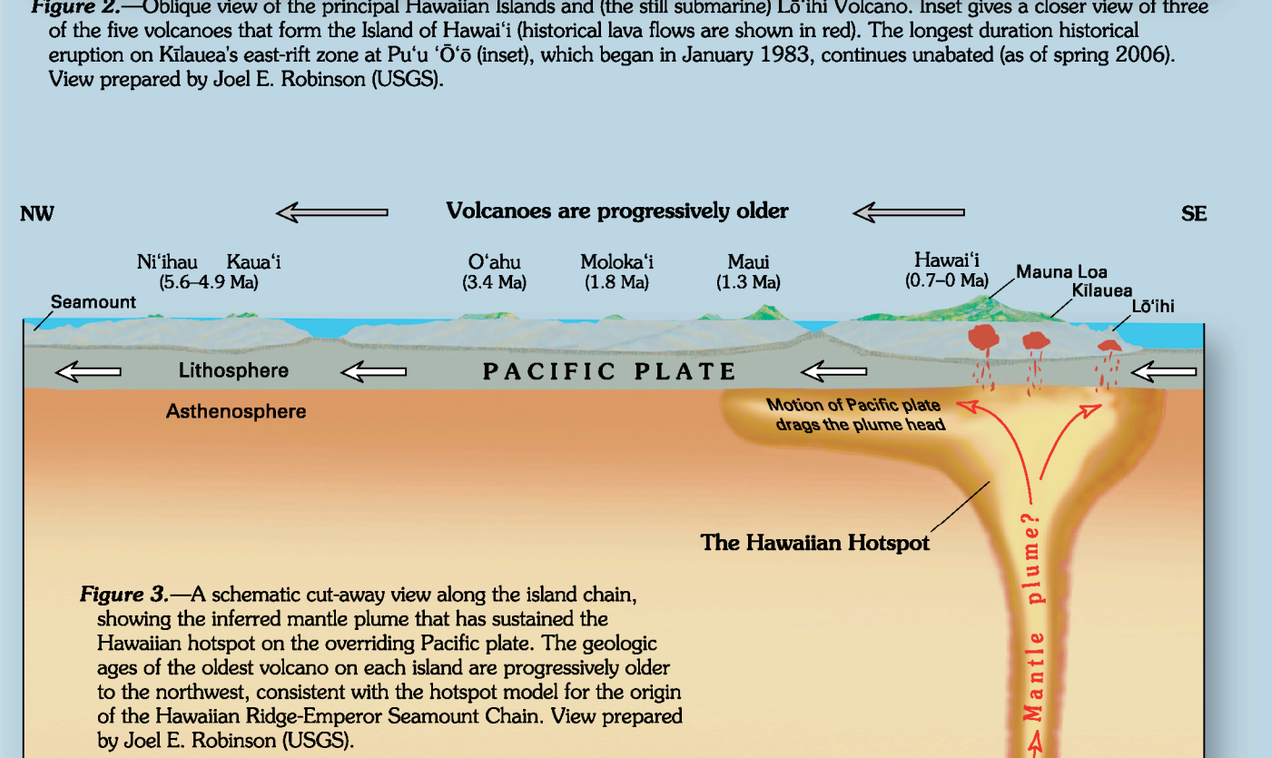

Figure 3.—A schematic cut-away view along the island chain, showing the inferred mantle plume that has sustained the Hawaiian hotspot on the overriding Pacific plate. The geologic ages of the oldest volcano on each island are progressively older to the northwest, consistent with the hotspot model for the origin of the Hawaiian Ridge-Emperor Seamount Chain. View prepared by Joel E. Robinson (USGS).

Most of Earth's active volcanoes are found along plate boundaries, but some occur within plate interiors. The best examples of such intraplate volcanoes are those of Hawaii, nearly 4,000 km from the nearest plate boundary (fig. 1). The Hawaiian Islands are the above-sea-level summits of volcanoes that form the southeastern end of the Hawaiian Ridge-Emperor Seamount Chain (figs. 1, 2). This 6,000-km-long, mostly submarine volcanic mountain range formed over the past 80 million years by the combined processes of magma formation, eruption, and movement of the Pacific plate over a mantle source—called a *melting anomaly* or *hotspot*— generally assumed to be relatively fixed in position. The sharp bend in the chain (fig. 1) is still not well understood despite intensive research. A recent explanation is that the northern segment (Emperor Seamount Chain) formed as the hotspot migrated southward until about 45 Ma, when its position became fixed. Then the northwesterly plate movement prevailed, forming the Hawaiian Ridge "downstream" from the hotspot.

Many scientists attribute the Hawaiian and some other hotspots to narrow plumes of hot, but not molten, material rising through the mantle (fig. 3). Partial melting of the mantle produces new magma that collects into blobs that rise through the overriding plate and ultimately erupt to form a new volcano on the sea floor. After many eruptions, the growing submarine volcano may emerge above sea level as an island volcano. Continued movement of the Pacific plate eventually carries each volcano away from the sustaining hotspot. Then, severed from their feeding magma sources, the eruptions ultimately cease. Even as a new volcano grows over the hotspot, it undergoes erosion. However, once eruptive activity stops, the volcano subsides as the plate cools and contracts, eventually sinking below sea level to form a flat-topped seamount. Recently active Hawaiian volcanoes—Kīlauea, Mauna Loa, and the present-day submarine but growing Lō'ihi (figs. 2, 3)—presumably still lie above, and are presently tapping, the Hawaiian hotspot. Midplate oceanic lavas are more fluid than those that build *stratovolcanoes* along convergent plate boundaries; they usually erupt nonexplosively, and some eruptions can last for decades (figs. 2, 4). Over geologic time, repeated outpourings of fluid lava, which can travel great distances from eruptive vents, form gently sloping *shield volcanoes* such as Hawaii's Mauna Loa (fig. 5).

Intraplate volcanism also occurs in continental interiors. For example, the Yellowstone Volcano (Yellowstone National Park) has produced three cataclysmic eruptions (fig. 6)—each associated with *caldera* collapse—during the past 2 million years. When an explosive eruption expels magma from a subsurface reservoir, the overlying volcano may collapse into the resulting void, leaving a shallow depression, or caldera, in place of the more familiar conically shaped volcano. Ash-fall deposits from these huge eruptions have been mapped thousands of kilometers from their source calderas (fig. 6). The Yellowstone volcanic plateau lies at the northeastern end of the Snake River Plain, a zone of geologically young (<17 Ma) volcanism that slashes across the Rocky Mountains, a mountain belt composed primarily of much older rocks (2,790–65 Ma). The geologic ages of the volcanic centers of the Snake River Plain are progressively older to the southwest (fig. 7). This age progression has been interpreted as resulting from volcanism associated with the passage of the North America plate over a Yellowstone hotspot, presumably sustained by a long-lived, relatively fixed, mantle plume. However, we emphasize that commonly held ideas such as rooting of thermal plumes deep in the mantle (>200 km) are topics of ongoing scientific debate. Yellowstone's most recent volcanic activity occurred about 70,000 years ago, but ground-deformation measurements indicate that the caldera is restless. The dynamics of its still-hot subsurface magmatic system are evident from its present-day spectacular expressions of geothermal energy, including Earth's most active geyser system (fig. 8).

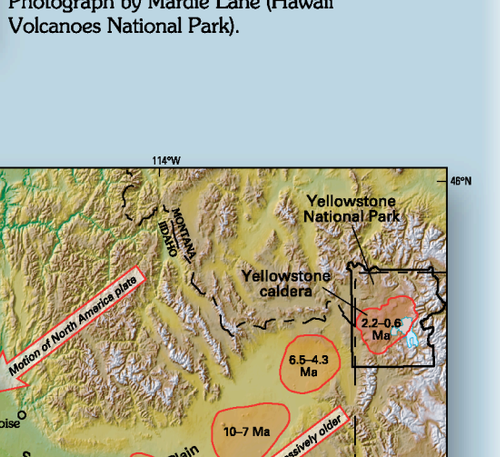

Figure 7.—Map showing the Yellowstone caldera and older volcanic centers (outlined in red). The southwest-trending alignment and age progression of these centers are thought to represent the "volcanic trail" of a continental hotspot fed by a mantle plume. Modified from Pierce and Morgan (1992, pl. 1.)

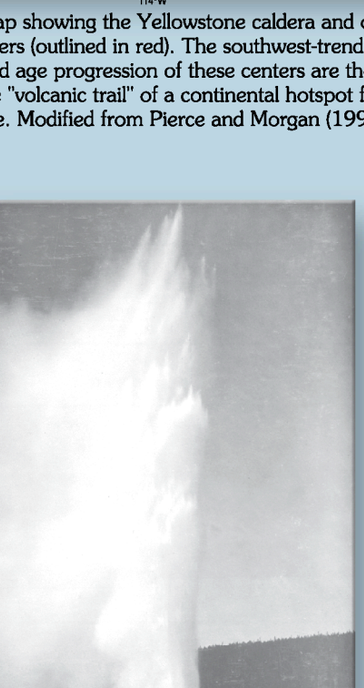

Figure 8.—Historic (1872) photograph, taken during the Hayden Survey, showing a towering fountain of water and steam jetting from Old Faithful Geyser in a region of Wyoming later designated as the first U.S. national park (Yellowstone). Its periodic, powerful bursts of geothermal energy continue to fascinate park visitors. Photograph by William Henry Jackson.

VI. Impacting Extraterrestrials Scar Planetary Surfaces

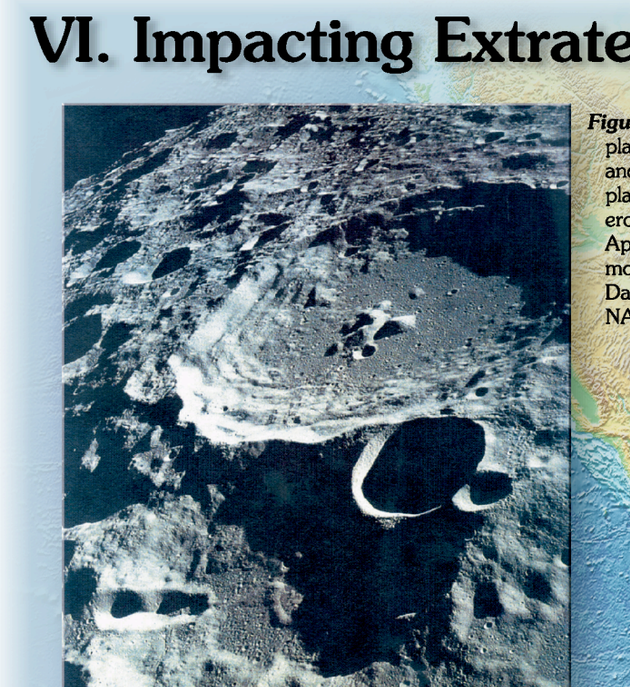

Figure 1.—Impact craters dominate barren planetary bodies that lack water, forests, ice, and sediment that hide them on Earth. Other planets also lack the post-impact tectonics and erosion that destroy craters on our planet. This Apollo 11 photograph shows part of our moon's far side. The largest crater shown, Daedalus, is 93 km in diameter. Image from NASA, no. AS11–44–6609.

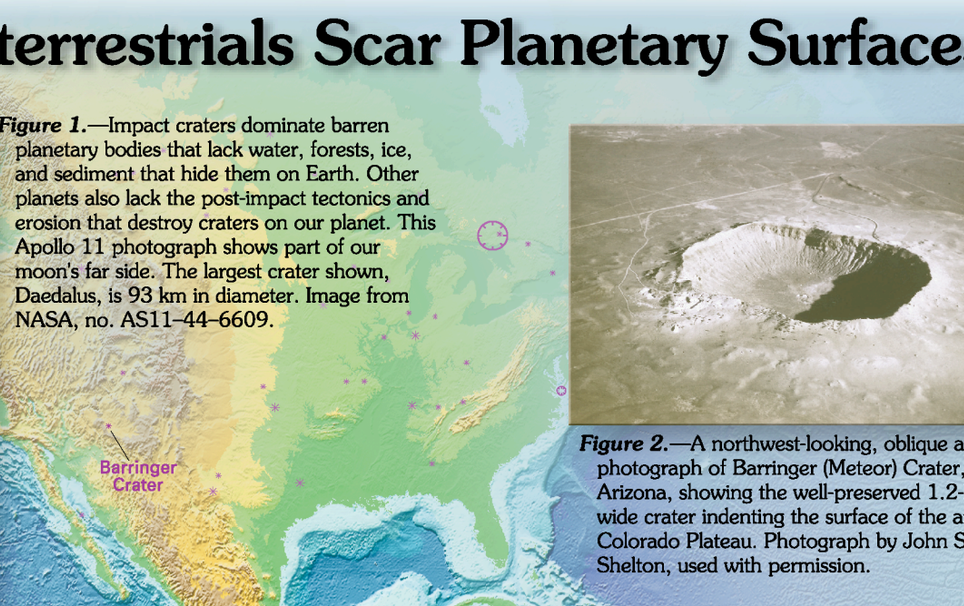

Figure 2.—A northwest-looking, oblique aerial photograph of Barringer (Meteor) Crater, Arizona, showing the well-preserved 1.2-km-wide crater indenting the surface of the arid Colorado Plateau. Photograph by John S. Shelton, used with permission.

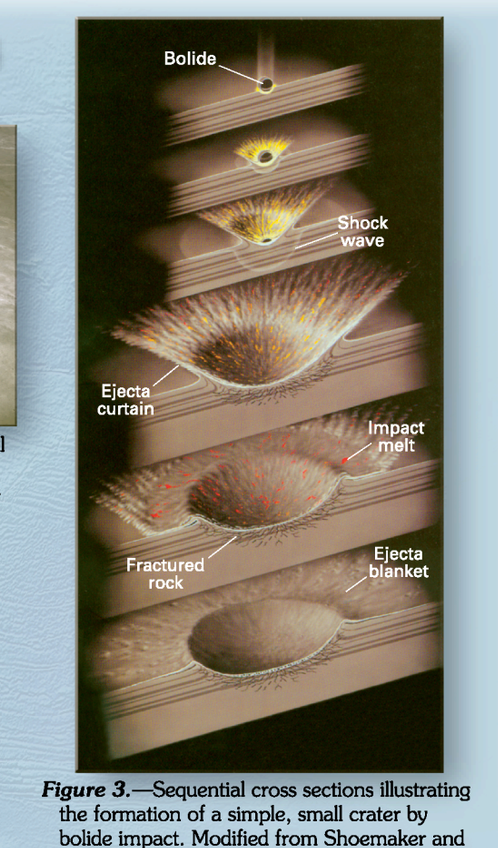

Figure 3.—Sequential cross sections illustrating the formation of a simple, small crater by bolide impact. Modified from Shoemaker and Shoemaker (1999). Used with permission of Cambridge University Press.

Crater formation by impact of extraterrestrial *bolides* (comets or asteroids) has been a significant process on the rocky moons and planets of our solar system and was particularly important during the first 500 million years of Earth's history (fig. 1). Although many small meteorites land on Earth every year, the fall of larger extraterrestrial fragments, forming giant impact craters, is (fortunately) infrequent. Evidence for large prehistoric impacts includes not only preserved crater shape and ejecta, but also mineralogic and structural changes caused by high-pressure shock waves. Nearly 170 terrestrial craters have so far been discovered, and they range widely in age (2,000 Ma to A.D. 1947). Their diameters can reach 300 km, and even larger craters may have been eroded away or covered by younger rocks.

One of the best-known and well-preserved craters is the Barringer (Meteor) Crater in Arizona, which was formed about 50,000 years ago (fig. 2). The incoming object is estimated to have measured about 50 m across and to have traveled at 65,000 km/hr (fig. 3). An impact crater this small might be formed somewhere on Earth every 1,000 years on average, whereas a 100-km-diameter crater might be produced once every 25 to 50 million years.

Most scientists—after lively debate—now accept the 1980 hypothesis that a bolide, ~10 km in diameter, impacted Earth 65 million years ago and was largely responsible for abrupt changes in the fossil record. These changes, including the extinction of dinosaurs, define the boundary between the Cretaceous and Tertiary Periods (commonly called the "K/T Boundary") of geologic time (see timeline below). The crater resulting from this impact is thought to be the now-buried 170-km-wide Chicxulub structure in Mexico (fig. 4). This impact involved a huge energy release, equivalent to that of an M13 earthquake, dwarfing the world's largest historical earthquake (M9.5, Chile, 1960).

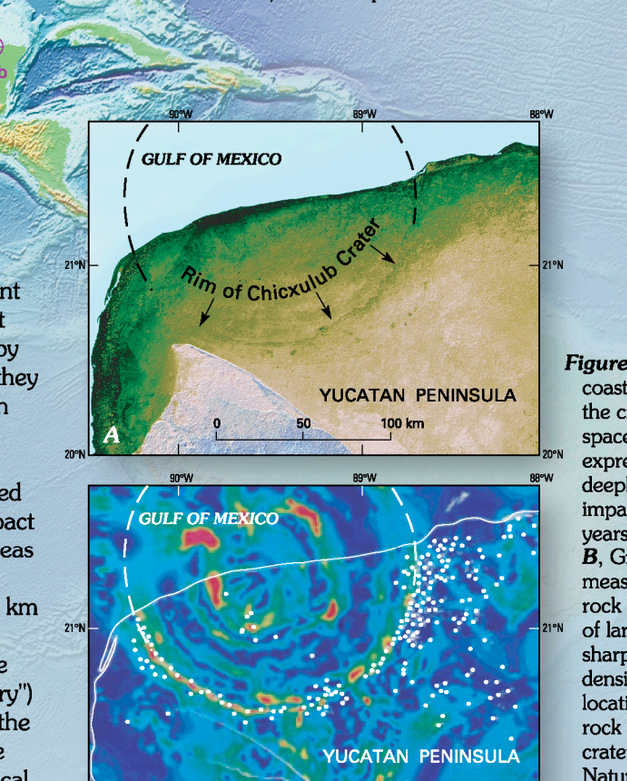

Figure 4.—Chicxulub impact crater, on the northern coast of Mexico's Yucatan Peninsula. Circular outline of the crater is indicated by dashed lines. *A*, View from space of the shallow (3- to 5-m-deep), subtle trough expressing the southern rim of the crater, which is deeply buried by younger sediments. The Chicxulub impact event caused widespread extinctions 65 million years ago. Image from NASA, no. PIA03379. *B*, Gravity-gradient map of the same area. Gravity measurements, processed to emphasize edges of dense rock bodies, reveal the multi-ring structure characteristic of large impact craters. Yellow to red colors indicate sharp boundaries between rock bodies of differing densities. White dots indicate surface sinkholes. Their locations reflect present-day ground-water flow along rock fractures influenced by Chicxulub's subsurface crater rim. Modified from Geological Survey of Canada, Natural Resources Canada, image on Web site http://miac.uqac.ca/

VII. Transform Faults—Where Plates Scrape Horizontally Past Each Other

Figure 1.—Map of California showing the main fault (heavy red line) and the less active strands (thin red lines) that together compose the San Andreas fault system. This system is part of a long, diffuse continental transform plate boundary that accounts for about 75 percent of the motion between the Pacific and North America plates (see fig. 2). USGS imagery enhanced by Joel E. Robinson.

Plates slide horizontally past each other along *transform* plate boundaries. Transforms occur both on land and in the ocean basins, linking spreading ridges and other plate boundaries. They typically produce shallow earthquakes, with accompanying ground faulting and generally little or no volcanic activity. Two well-known continental examples are the North Anatolian fault (Turkey) and the San Andreas fault system (California). The San Andreas system is a family of related faults in a *diffuse plate boundary zone* (see interpretive map of plate tectonics, on front); this and similarly broad zones elsewhere also can be described as consisting of one or more *microplates*. Although most of the motion between the North America and Pacific plates occurs along the San Andreas fault itself, substantial movements also involve many smaller faults in a wide zone from western Nevada to offshore California (figs. 1, 2). Sudden movements within this system have produced many damaging earthquakes, including the famous M7.8 San Francisco shock of 1906 (fig. 3), the M7.1 Imperial Valley earthquake of 1940 (fig. 4), and the M6.7 Northridge jolt of 1994 (table 3, no. 23).

The surface expressions of continental transform plate boundaries depend largely on the orientation of the boundary in relation to the direction of plate motion across the boundary. For the San Andreas system, faults that veer to the left (or to the west when looking north) of the direction of Pacific plate motion produce compressive (squeezing) deformation and uplift, thus forming mountains such as the Transverse Ranges in southern California (figs. 1, 2). This deformation also splinters the western fringe of the North America plate, forming a microplate extending from the San Andreas fault to smaller faults east of the Sierra Nevada. Conversely, fault segments that veer to the right cause extensional ("pull-apart") deformation and subsidence, producing topographic lows, such as the Salton Sea in southern California (figs. 1, 2). Strands of the San Andreas fault with trends that more closely parallel plate motion directions show smaller scale features, such as offsets of stream channels (fig. 5) or rows of trees (fig. 4). Natural or manmade features also can be shifted by slow fault movements (*fault creep*), rather than by sudden lurches associated with earthquakes.

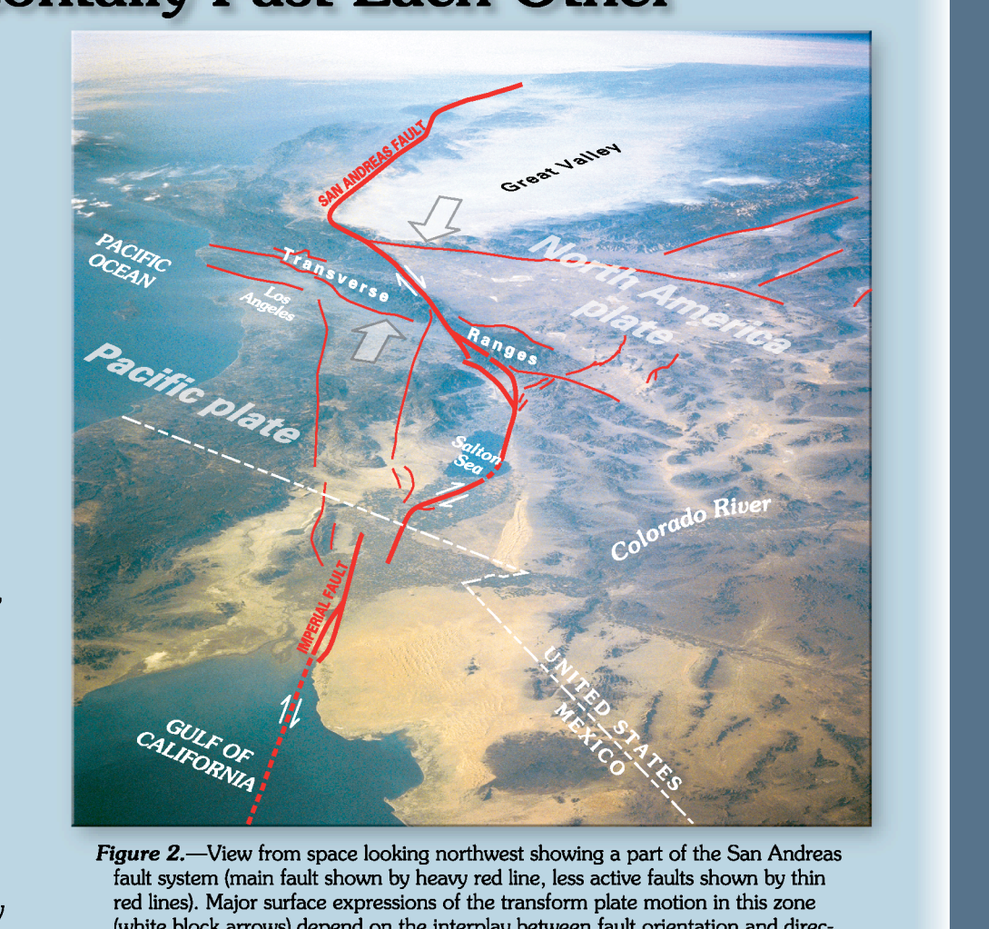

Figure 2.—View from space looking northwest showing a part of the San Andreas fault system (main fault shown by heavy red line, less active faults shown by thin red lines). Major surface expressions of the transform plate motion in this zone (white block arrows) depend on the interplay between fault orientation and direction of plate motion. Image from NASA, no. STS103–701–39; faults drawn by Michael Rymer (USGS).

Figure 3.—View of fire down Sacramento Street in San Francisco showing building damage caused by the earthquake of 1906. Smoke in background is from approaching fires that were ultimately more damaging than the shaking itself. Photograph by Arnold Genthe (American 1869–1942); silver gelatin print; image 200 x 329 mm (7⅞ x 12¹⁵⁄₁₆ in). Courtesy of Fine Arts Museums of San Francisco, Museum Collection A046248.

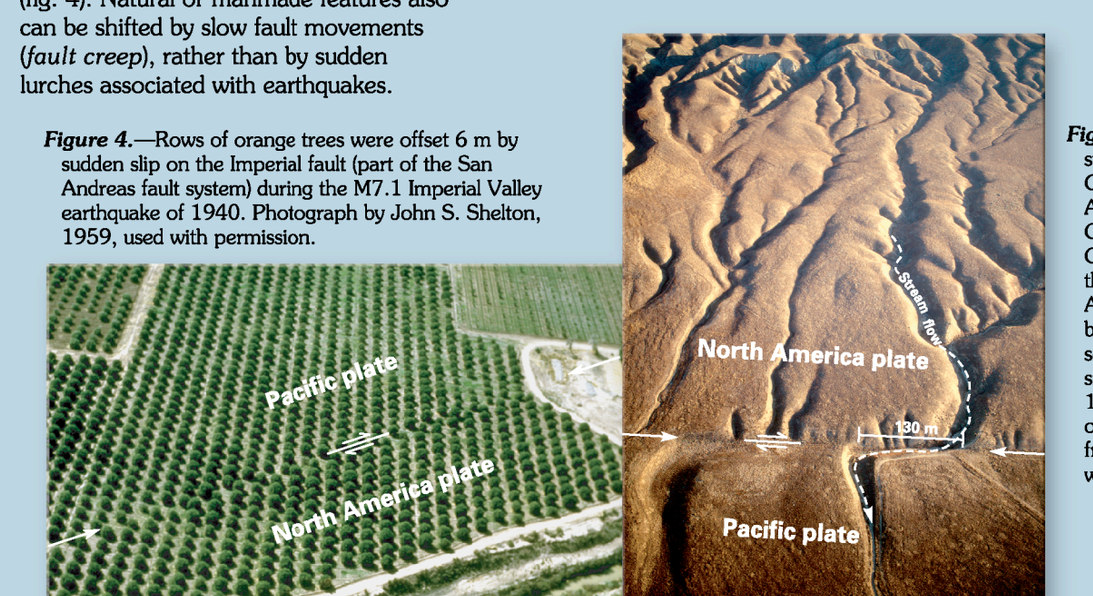

Figure 4.—Rows of orange trees were offset 6 m by sudden slip on the Imperial fault (part of the San Andreas fault system) during the M7.1 Imperial Valley earthquake of 1940. Photograph by John S. Shelton, 1959, used with permission.

Figure 5.—Aerial view of the stream channel of Wallace Creek offset by San Andreas fault motion on the Carrizo Plain, central California. The fault shifted the creek on the North America plate to the right by 130 m over a period of several thousand years. A single great earthquake in 1857 caused about 9.5 m of this motion. Photograph from Collier (1999), used with permission.

REFERENCES CITED

Bird, Peter, 2003, An updated digital model of plate boundaries: Geochemistry, Geophysics, Geosystems, v. 4, no. 3, 52 p., available only online at http://www.agu.org/journals/gc/ gc0303/2001GC000252/

Bouysse, Philippe, and others, 2000, Geological map of the world (Carte géologique du monde) (2d ed.): Paris, Commission for the Geological Map of the World and UNESCO, 3 sheets, scale 1:25,000,000. (In English and French. Also available on CD-ROM.)

Carbotte, S.M., and Scheirer, D.S., 2004, Variability of ocean crustal structure created along the global mid-ocean ridge, *in* Davis, Earl, and Elderfield, Harry, eds., Hydrogeology of the oceanic lithosphere: Cambridge, United Kingdom, Cambridge University Press, p. 59–107.

Collier, Michael, 1999, A land in motion; California's San Andreas fault: Berkeley, University of California Press, 128 p.

DeMets, Charles, Gordon, R.G., Argus, D.F., and Stein, Seth, 1994, Effect of recent revisions to the geomagnetic reversal time scale on estimates of current plate motions: Geophysical Research Letters, v. 21, no. 20, p. 2191–2194.

Engdahl, E.R., and Villaseñor, Antonio, 2002, Global seismicity: 1900–1999, *in* Lee, W.H.K., Kanamori, Hiroo, Jennings, P.C., and Kisslinger, Carl, eds., International handbook of earthquake and engineering seismology, Part A: Boston, Academic Press, p. 665–690.

Goodwin, A.M., 1991, Precambrian geology; The dynamic evolution of the continental crust: London, Academic Press, 666 p.

Gordon, R.G., 2000, Diffuse oceanic plate boundaries; Strain rates, vertically averaged rheology, and comparisons with narrow plate boundaries and stable plate interiors, *in* Richards, M.A., Gordon, R.G., and van der Hilst, R.D., eds., The history and dynamics of global plate motions: American Geophysical Union Geophysical Monograph 121, p. 143–159.

Grieve, R.A.F., 1998, Extraterrestrial impacts on Earth; The evidence and the consequences, *in* Grady, M.M., Hutchison, R., McCall, G.J.H., and Rothery, D.A., eds., Meteorites; Flux with time and impact effects: Geological Society [of London] Special Publication 140, p. 105–131.

Izett, G.A., and Wilcox, R.E., 1982, Map showing localities and inferred distributions of the Huckleberry Ridge, Mesa Falls, and Lava Creek ash beds (Pearlette family ash beds) of Pleistocene age in the western United States and southern Canada: U.S. Geological Survey Miscellaneous Investigations Series Map I–1325, scale 1:4,000,000.

Kárason, Hrafnkell, and van der Hilst, R.D., 2000, Constraints on mantle convection from seismic tomography, *in* Richards, M.A., Gordon, R.G., and van der Hilst, R.D., eds., The history and dynamics of global plate motions: American Geophysical Union Geophysical Monograph 121, p. 277–288. Copyright 2000 American Geophysical Union.

Kious, W.J., and Tilling, R.I., 1996, This dynamic Earth; The story of plate tectonics: Reston, Va., U.S. Geological Survey General Interest Publication, 77 p. (Also available online at http://pubs.usgs.gov/publications/text/dynamic.html)

Müller, R.D., Roest, W.R., Royer, J.-Y., Gahagan, L.M., and Sclater, J.G., 1997, Digital isochrons of the world's ocean floor: Journal of Geophysical Research (Solid Earth and Planets), v. 102, no. B2, p. 3211–3214. Copyright 1997 American Geophysical Union.

Pearce, Julian, 2002, The oceanic lithosphere: JOIDES Journal, v. 28, no. 1, p. 61–66.

Pierce, K.L., and Morgan, L.A., 1992, The track of the Yellowstone hot spot; Volcanism, faulting, and uplift, chap. 1 *of* Link, P.K., Kuntz, M.A., and Platt, L.B., eds., Regional geology of eastern Idaho and western Wyoming: Geological Society of America Memoir 179, p. 1–53, 1 oversize pl.

Scotese, C.R., 2001, Digital paleogeographic map archive on CD-ROM (PALEOMAP Project): Arlington, Tex., 1 disc.

Shoemaker, E.M., and Shoemaker, C.S., 1999, The role of collisions, chap. 6 *of* Beatty, J.K., Petersen, C.C., and Chaikin, Andrew, The new solar system: New York, Cambridge University Press, p. 69–86.

Simkin, Tom, Unger, J.D., Tilling, R.I., Vogt, P.R., and Spall, Henry, 1994, This dynamic planet; World map of volcanoes, earthquakes, impact craters, and plate tectonics: U.S. Geological Survey, scale 1:30,000,000. (Also available online at http://pubs.usgs.gov/pdf/planet.html)

U.S. Geological Survey, 1997, GTOPO30: U.S. Geological Survey Web site, available at http://edcdaac.usgs.gov/gtopo30/gtopo30.asp (accessed June 11, 1997).

Zhao, Dapeng, Hasagawa, Akira, and Horiuchi, Shigeki, 1992, Tomographic imaging of *P* and *S* wave velocity structure beneath northeastern Japan: Journal of Geophysical Research (Solid Earth and Planets), v. 97, no. B13, p. 19,909–19,928.

SELECTED REFERENCES

Bamber, J.L., Layberry, R.L., and Gogenini, S.P., 2001, A new ice thickness and bed data set for the Greenland ice sheet: Journal of Geophysical Research (Atmospheres), v. 106, no. D24, p. 33,773–33,788.

Cormier, Marie-Hélène, Ryan, W.B.F., Shah, A.K., Jin, Wen, Bradley, A.M., and Yoerger, D.R., 2003, Waxing and waning volcanism along the East Pacific Rise on a millennium time scale: Geology, v. 31, no. 7, p. 633–636.

Cox, Allan, and Hart, R.B., 1986, Plate tectonics; How it works: Palo Alto, Calif., Blackwell Scientific Publications, 392 p.

Decker, Robert, and Decker, Barbara, 1998, Volcanoes (3d ed.): New York, W.H. Freeman and Company, 320 p.

Foulger, G.R., Natland, J.H., Presnall, D.C., and Anderson, D.L., eds., 2005, Plates, plumes, and paradigms: Geological Society of America Special Paper 388, 881 p.

French, B.M., 1998, Traces of catastrophe; A handbook of shock-metamorphic effects in terrestrial meteorite impact structures: Houston, Tex., Lunar and Planetary Institute, LPI Contribution No. 954, 120 p.

Gripp, A.E., and Gordon, R.G., 2002, Young tracks of hotspots and current plate velocities: Geophysical Journal International, v. 150, no. 2, p. 321–361.

Hough, S.E., 2002, Earthshaking science; What we know (and don't know) about earthquakes: Princeton, N.J., Princeton University Press, 238 p.

Jakobsson, Martin, Grantz, Arthur, Kristoffersen, Yngve, and Macnab, Ron, 2003, Physiographic provinces of the Arctic Ocean seafloor: Geological Society of America Bulletin, v. 115, p. 1443–1455.

Johnston, A.C., 1996, Seismic moment assessment of earthquakes in stable continental regions-II. Historical seismicity: Geophysical Journal International, v. 125, p. 639–678.

Kearey, Philip, and Vine, F.J., 1996, Global tectonics (2d ed.): Oxford, Blackwell Science Ltd., 333 p.

Kleinrock, M.C., and Humphris, S.E., 1996, Structural asymmetry of the TAG rift valley; Evidence from a near-bottom survey for episodic spreading: Geophysical Research Letters, v. 23, no. 23, p. 3439–3442.

Lee, W.H.K., Kanamori, Hiroo, Jennings, P.C., and Kisslinger, Carl, eds., International handbook of earthquake and engineering seismology, Part A: Boston, Academic Press, 933 p.

Luhr, J.F., ed., 2003, Earth: New York, Dorling Kindersley, 520 p.

Palmer, A.R., 1989, The Earth has a history: Boulder, Colo., Geological Society of America, 20-minute videocassette with 7-p. supplemental teacher's manual.

Redfern, Ron, 2001, Origins; The evolution of continents, oceans, and life: Tulsa, University of Oklahoma Press, 360 p.

Scotese, C.R., 2001, Paleogeography, v. 1 *of* Atlas of Earth history (PALEOMAP Project): Arlington, Tex., 52 p. (Available online at http://www.scotese.com/)

Siebert, Lee, and Simkin, Tom, 2002–, Volcanoes of the world; An illustrated catalog of Holocene volcanoes and their eruptions: Smithsonian Institution, Global Volcanism Program Digital Information Series GVP–3. (Available online at http://www.volcano.si.edu/world/)

Sigurdsson, Haraldur, ed., 2000, Encyclopedia of volcanoes: San Diego, Academic Press, 1417 p.

Simkin, Tom, and Siebert, Lee, 1994, Volcanoes of the world; A regional directory, gazetteer, and chronology of volcanism during the last 10,000 years: Phoenix, Ariz., Geoscience Press, 368 p.

Smith, W.H.F., and Sandwell, D.T., 1997, Global sea floor topography from satellite altimetry and ship depth soundings: Science, v. 277, p. 1957–1962.

Stein, Seth, and Wysession, Michael, 2003, An introduction to seismology, earthquakes, and Earth structure: Malden, Mass., Blackwell Science, 498 p.

Suggested citation: Simkin, Tom, Tilling, R.I., Vogt, P.R., Kirby, S.H., Kimberly, Paul, and Stewart, D.B., 2006, This dynamic planet; World map of volcanoes, earthquakes, impact craters, and plate tectonics: U.S. Geological Survey Geologic Investigations Series Map I–2800, 1 two-sided sheet, scale 1:30,000,000.

For sale by U.S. Geological Survey, Information Services, Box 25286, Federal Center, Denver, CO 80225; telephone 1-888-ASK-USGS; World Wide Web: http://www.usgs.gov/

Printed in the USA by The Pikes Peak Lithographing Co.

Conversions and Abbreviations

Multiply	By	To obtain
Millimeter (mm)	0.03937	Inch (in)
Centimeter (cm)	0.39370	Inch (in)
Meter (m)	3.281	Foot (ft)
Kilometer (km)	0.6214	Mile (mi)
Square kilometer (km²)	0.3861	Square mile (mi²)
Cubic kilometer (km³)	0.23992	Cubic mile (mi³)

Diameter (D) — Mega-annum (Ma) million years ago
Magnitude (M) — mm/yr = km/Ma

EARTH'S LONG LIFE HISTORY

The maps to the right show one scientific interpretation of Earth's many changes—in locations of continents, sea level, and global climate—through geologic time. These maps, together with the geologic timeline below, emphasize that the dynamic processes illustrated on the main map and elaborated above have been operating for hundreds of millions of years and will continue far into the future. Maps modified from Scotese (2001); timeline data from multiple sources (see http://www.minerals.si.edu/tdpmap).